Research Square

Preprints are preliminary reports that have not undergone peer review.
They should not be considered conclusive, used to inform clinical practice,
or referenced by the media as validated information.

The synergistic effect of sepiolite-LDH hybrid nanofiber and phytic-based nanosheet towards improving the fire retardancy, heat resistance, and mechanical properties of epoxy resin

Su-Hua Zhang
Southwest University of Science and Technology
Zhen-Zhong Wu
Southwest University of Science and Technology
Shi-Hu Han
Southwest University of Science and Technology
Yi-Qing Wang
Southwest University of Science and Technology
Li-Jun Qian
China Light Industry Engineering Technology Research Center of Advanced Flame Retardants, Beijing Technology and Business University
Xiao-Ping Hu (huxiaoping@swust.edu.cn)
Southwest University of Science and Technology

Research Article

Keywords: Epoxy, Fire retardance, Thermal stability, Mechanical strength, Synergistic Mechanism

Posted Date: September 30th, 2022

DOI: https://doi.org/10.21203/rs.3.rs-2028707/v1

License: This work is licensed under a Creative Commons Attribution 4.0 International License.
Read Full License

Abstract

Usually, it is difficult to achieve satisfactory fire retardancy of epoxy resin at low addition by adding inorganic nano-fillers alone. Herein, sepiolite nanofibers loaded with layered double metal hydroxide (a-SEP@LDH) and P/N-containing flame retardant nanosheet (PAMA) were prepared via hydrothermal method, respectively. The UL-94 V-0 rating and an LOI value of 31.6% were achieved for EP by loading 1wt% a-SEP@LDH and 2wt% PAMA. Compared to adding sole a-SEP@LDH, the thermal stability of EP/a-SEP@LDH/PAMA was improved significantly, the total heat release (THR) and peak heat release rate (pHRR) decreased by 10.2% and 28.8%, respectively. Additionally, the total CO_2 production decreased by 12.5% and the char residue yield increased to 19.9wt%. Moreover, the tensile strength and impact strength of the EP composites were remarkably improved owing to the incorporation of PAMA. To sum up, this work provides an environmentally benign, low-cost and efficient way for EP to achieve outstanding fire retardance, excellent thermal stability and high mechanical properties at a low addition.

1 Introduction

Epoxy resin (EP) is widely used in coatings, electronics, construction and industrial fields, owning to its excellent mechanical properties, adhesion, electrochemical insulation and corrosion resistance [1–3]. However, its inherent flammability restricts the extensive applications where high fire requirement are required. Researchers are generally devoted to imparting the required fire retardancy of EP by incorporating additive flame retardants or copolymerizing with reactive flame retardants [4–6]. Adding flame retardants to epoxy resin is a convenient and common method, including inorganic filler [7], intumescent flame retardant [8], silicon-based flame retardant [9]. However, additive flame retardants will deteriorate the mechanical strength and thermal resistance of EP owing to its high loading amount [10, 11], Therefore, it is absolutely essential to develop an eco-friendly flame retardant to balances the comprehensive performances of EP composite.

In our previous work, a novel one-dimensional (1D) inorganic nanofiller (a-SEP@LDH) was prepared by the self-assembly of Ni-Fe LDH on the surface of acidified sepiolite nanofibers (a-SEP) [12]. By introducing 2.3wt% a-SEP@LDH into EP, the thermostability and tensile strength were improved. However, only UL-94 V-1 rating was achieved, the reason may be attributed to the lower catalytic carbonization effect of a-SEP@LDH, namely, a-SEP@LDH used alone is not able to produce enough swelling char layer and then put out the flame promptly. It can be verified by the slight increasement of char residue of EP/a-SEP@LDH in cone testing from 12.0wt% of EP to 14.9wt%. Therefore, employing a P/N-containing intumescent flame retardant as synergist is a potential strategy to enhance the charring ability of EP/a-SEP@LDH system, thus improving the fire retardancy.

The traditional P/N-containing intumescent flame retardants (IFR) shows good flame retardancy, however, there are some disadvantages such as poor dispersion and easy agglomeration [13]. The synthesis of a “three-in-one” IFR with two-dimensional (2D) supramolecular nanostructure is beneficial to improve the comprehensive properties of EP due to the barrier effect of its nanosheet structure and more

contact area with the polymer matrix. Our group has reported a novel 2D hyperbranched melamine phytate nanosheet (PAMA) [14], which required 6wt% addition in epoxy resins to obtain a UL-94 V-0 rating, and its total smoke production (TSP) is 37% lower than those of pure EP, the char residue yield increase to 26.7% from 4.4% of EP. Qin et al. synthesized a 2D melamine trimetaphosphate (MAP), the addition of 4% MAP increased the LOI value of EP to 30.0% and a UL-94 V-0 rating attained. Meanwhile its peak of heat release rate (pHRR) and total smoke production (TSP) decrease by 65.6% and 45.4% respectively [15]. The above results show that P/N-containing 2D flame retardant do have excellent smoke suppression and carbonization effect, which can be employed to synergistic boost fire retardant capability of inorganic nano fillers.

Hence, in this study, combining 2D nanosheet PAMA and 1D hybrid nanofiber a-SEP@LDH, the synergistic effect of their co-adding to EP on fire retardancy, thermal stability and mechanical properties at low addition amount was analyzed. Moreover, the fire retardant and strengthening mechanism of EP composites were comprehensively discussed as well.

2 Experimental Section

2.1 Materials

Melamine (MA, chemically pure), phytic acid (PA, biochemical reagent, 70% aqueous solution), nickel nitrate hexahydrate, iron nitrate nonahydrate, sodium hydroxide (NaOH), 4,4-diaminodiphenylmethane (DDM) and ethanol were obtained from Sinopharm Chemical Reagent Co., Ltd. (Shanghai, China). Hydrochloric acid (HCl) and sodium hexametaphosphate (SHMP) were provided by KeLong Chemical Reagent Co., Ltd. (Chengdu, China). Raw sepiolite (SEP) was purchased from Neixiang Dongfeng Sepiolite Limited Liability Company (Neixiang, China). Epoxy resin of bisphenol A diglycidyl ether (DGEBA, E44, epoxy value of 0.43–0.47 mol/100g) was purchased from Nantong XingChen Synthetic Materials Co., Ltd. (Nantong, China).

2.2 Preparation of a-SEP@LDH

The a-SEP@LDH was prepared by hydrothermal assisted coprecipitation as described in previous literature [12]. In short, a certain amount of raw sepiolite (r-SEP) was firstly dispersed in the aqueous solution for 30min, then filtered the above suspension solution. The obtained filtered cake was added in the SHMP aqueous solution successively and stirred for 30 min. After standing for 2h, the pretreated sepiolite was obtained by filtering, washing and dried. Next, the pretreated sepiolite was dispersed in 5mol/L HCl solution and continuously stirred at 80°C for 24h. The acidified sepiolite (a-SEP) solids were collected by filtered, washed with deionized water until completely removed chloridion, subsequently dried in vacuum oven at 80°C.

1g a-SEP was added in 100ml deionized water and ultrasonic agitated for 0.5h, whereafter, the mixed nitrate solution containing nickel and iron (the molar ratio of Ni^{2+} and Fe^{3+} was fixed at 3:1, the mass ratio of sepiolite and Fe $(NO_3)_3 \cdot 9H_2O$ was controlled at 1:2) was added dropwise to the a-SEP

suspension, and the pH value was adjusted to 9–10 with 5mol/L NaOH aqueous solution. The obtained yellow solution was mechanically stirred at room temperature for 24 hours, afterwards transferred to 500ml teflon lined autoclave and aged for 36h at 120°C. The resulting product (a-SEP@LDH) was cooled to room temperature, filtered and washed several times, then dried to constant weight at 70°C.

2.3 Synthesis of PAMA

PAMA was synthesized by hydrothermal process according to our previous report [14]. 30.24g melamine (MA) was dispersed in 400ml deionized water and mechanically stirred until uniformly dispersed at room temperature. Then the phytic acid aqueous solution (0.2mol/L) was dripped into the MA solution and stirred for 0.5h. Thereafter, the obtained white emulsion was transferred into 1000ml teflon lined autoclave and aged for 48h at 80°C. After autoclave was cooled to room temperature, the final product was filtered and repeatedly washed with deionized water. In the end, the resulting white powder (PAMA) was obtained by vacuum drying at 70°C and grinding.

2.4 Preparation of EP composites

The EP composites was prepared by casting method. The composition of EP samples is listed in Table 1. First, 24g E44 was placed in a 250ml three-neck flask and mechanically stirred at 110°C, then 50 ml of ethanol dispersion solution involving a certain amount of PAMA and a-SEP@LDH powder was added into EP matrix and stirred continually for 6h under vacuum. Subsequently, pre-melted DDM (the molar ratio of epoxy monomer to DDM is 4:1) was poured into the above mixture, which was transferred to a polytetrafluoroethylene mold after stirring 10min at 90°C. Finally, the mixture was cured at 120°C for 3h and re-cured at 150°C for 2h, the prepared samples were labelled as EP/a-SEP@LDH/PAMA. The detailed preparation route is depicted in Scheme 1. What is more, the preparation process for EP, EP/PAMA, and EP/a-SEP@LDH is the same as the above process.

Scheme 1 Preparation route of EP composites

2.5 Characterization

Fourier transform infrared (FTIR) spectroscopy tests were performed using one spectrometer of American PE (Perkin Elmer) instrument company, and the scanning range is 4000 cm^{-1} to 400 cm^{-1}.

The X-ray diffraction pattern (XRD) was measured by D/MAX-1400 rotating anode X-ray diffractometer (rigaku, Japan) with a Cu-K_α radiation (λ = 0.1541 nm), the scanning speed and scanning range were 3º/min and 3–30º / 70º, respectively.

The thermogravimetric analysis (TG) was performed on a Jupiter STA449C synchronous thermal analyzer (Netzsch, Germany). The samples were heated from 30ºC to 800 ºC at a heating rate of 10 ºC/min in N_2 atmosphere

The vertical burning tests (UL-94) were carried out using the M607 horizontal vertical burning tester (Qingdao Shanfang Instrument Co., Ltd., China) according to ASTM D3801, and the sample dimension

was 130×13×3.2mm^3.

The limiting oxygen index (LOI) was obtained by a JF-3 oxygen index tester (Nanjing Jionglei Instrument Equipment Co., Ltd., China) according to ASTM D2863-97, and the sample size was 100×6.5×3.2mm^3.

The cone calorimetry test (CCT) was measured according to ISO 5660 (Fire Testing Technology, UK). The size of samples was 100×100×4 mm^3 under an external heat flux of 35 Kw/m^2.

The emission scanning electron microscopy (SEM) with an energy dispersive spectroscopy (EDS) was implemented on the Ultra55 Germany Carl zeiss NTS Gmbh.

The glass transition temperature (T_g) was conducted on differential scanning calorimetry (DSC) using a DSCQ2000 (TA Instrument company, UK).

The tensile properties of all samples were tested with a rate of 2 mm/min, according to GB/T1040.3–2006.

The non-notched impact tests of all samples were measured according to GB/T1040.3–2008 with dimensions of 80×10×4 mm^3.

3 Results And Discussion

3.1. Characterization of PAMA and a-SEP@LDH

The FTIR spectra of PAMA and a-SEP@LDH are presented in Fig. 1a and b. In Fig. 1a, the multi-absorption peaks at 3469cm^{-1}, 3419cm^{-1}, 3333cm^{-1}, 3132cm^{-1} in MA are attributed to stretching vibration of -NH_2 [16], the bending vibration of -NH_2 appears at 1652cm^{-1}, the peaks at 1552cm^{-1}, 1438cm^{-1} and 851cm^{-1} are corresponding to the skeleton vibration of triazine ring [17]. For PAMA, the broad absorption band at 3360cm^{-1} is assigned to the stretching vibration of N-H and -OH. The broad band at 3141cm^{-1} is assigned to the overlay of -NH_3^+ stretching vibration and partially unreacted -NH_2 [14]. In addition, the vibration absorption of -NH_3^+ also appeared at 1509cm^{-1} [16]. The bending vibration of -NH_2 of MA shifts to 1675 cm^{-1} in PAMA, which is due to the intermolecular interactions between the -NH_2 and -OH [18]. All the vibrations of triazine ring shifts to 1396cm^{-1} and 778cm^{-1}, owing to the hydrogen bond effect between MA and PA, and the deformation of triazine ring in the self-assembly process of nanosheet [19]. Furthermore, a series of peaks appear at 1675cm^{-1}, 1176cm^{-1}, 1064cm^{-1}, 982cm^{-1}, 519cm^{-1} belong to bending vibration of OH in P-OH, stretching vibration of P = O bond, asymmetric vibration of PO_3^{2-} and the stretching and bending vibrations of P-O bond [20, 21], respectively. These characteristic peaks prove that the successfully protonation of amino group in MA and the occurrence of the neutralization reaction with PA. In Fig. 1b, the two absorption peaks at 3675cm^{-1} and 745cm^{-1} of a-SEP are associated to the stretching and bending vibrations of Mg-OH [22]. The band located at 3448cm^{-}

^{1} and 1637cm^{-1} are originated from stretching and deformation vibrations of -OH in crystal water [23]. Moreover, the broad absorption peak at about 1000cm^{-1} and the peak at 456cm^{-1} belong to the Si-O-Si groups [24]. For LDH, the typical peak at 1384cm^{-1} is attributed to NO_3^-, and a broad peak around 643cm^{-1} corresponds to the lattice vibration of Ni-O-Fe [25]. On the FTIR of a-SEP@LDH, all the typical peaks of LDH still exist. Meanwhile, the Si-O-Si bonds of a-SEP at 1000cm^{-1} and 456cm^{-1} are also observed. The absorption peaks at 3675cm^{-1} and 745cm^{-1} associated with Mg-OH almost disappear, which is due to that the partial Mg^{2+} has been replaced by Ni^{2+} and Fe^{3+} [26], indicating a-SEP and LDH are assembled not only through electrostatic interaction but also through chemical binding.

The morphology of PAMA, a-SEP and a-SEP@LDH was observed by SEM. PAMA shows a nano sheet structure with the average transverse diameter of less than 5μm and the thickness of about 50nm (Fig. 2a). The a-SEP exhibits a smooth fiber-like structure and a diameter of around 50nm (Fig. 2b). Compared with a-SEP, the surface of the hybrids becomes rough after the formation of Ni-Fe LDH (Fig. 2c), which is mainly caused by the electrostatic absorption due to the negative charge of a-SEP and positive charge of LDH.

The XRD patterns of the PAMA and a-SEP@LDH are displayed in Fig. 3. In Fig. 3a, the diffraction peaks of MA are in good agreement with structures indexed by JCPDS No.24-1654, illustrating that MA is a monoclinic crystal. There are a series of new diffraction peaks for PAMA at 8.56°, 14.48,° 15.28°, 16.7°, 18.16°, 18.75°, 27.57°, 28.05°in contrast to MA, and these reflection peaks belong to ammonium phosphate hydrate (PDF#81-1753), indicating that the crystal structures of PAMA and MA are completely different. The characteristic diffraction peak at 8.56° is due to the layered structure of PAMA formed by the neutralization of melamine and phytic acid [27]. What is more, the reflection peak at 27.57°is formed by the π-π stacking of triazine rings [20], corresponding to an inter-planar spacing of 0.3233nm according to the Bragg equation. As for Fig. 3b, the diffraction characteristic peaks at 11.18° and 22.41° correspond to the (003) and (006) crystal planes of Ni-Fe LDH structure [28]. The (003) reflection of LDH shows a basal spacing of 0.79nm, demonstrating that the interlayer anion is NO_3^- [29]. The weak characteristic absorption peaks of a-SEP exist in a-SEP@LDH infers that Ni-Fe LDH has been successfully assembled on the surface of a-SEP fibers.

The thermal stability of PAMA, a-SEP@LDH and mixed powder (the mass ratio of PAMA and a-SEP@LDH is 2:1) had been investigated by the TG and DTG curves in N_2 atmosphere and the results are presented in Fig. 4 and Table 1. The thermal weight loss of PAMA can be divided into four stages, and the peak value of each stage is reached at 83.2°C, 258.5°C, 390.0°C and 551.6°C, respectively. The mass loss from room temperature to 140°C is due to the loss of physically adsorbed water on the surface of PAMA, and the thermal-degradation between 185°C and 310°C is caused by the decomposition of unstable structural groups and the release of NH_3 and H_2O, the third thermal decomposition stage occurs range from 350°C to 430°C, and the temperature at maximum weight loss rate (T_{max}) appears at about 390°C, mainly due to the generation of ammonium polyphosphate and ammonium metaphosphate formed by the thermal decomposition of melamine and the dehydration and cross-linking of the phytic acid [14, 30]. The last

degradation step, in the range of 510°C to 620°C, corresponding to the formation of metaphosphoric acid, polyphosphoric acid and phosphoric acid via the further degradation of phosphate [31, 32]. Regarding to a-SEP@LDH, the mass loss below 200°C is attributed to the removal of adsorbed water. When the temperature is higher than 200°C, the elimination of the zeolite water and the coordination crystal water occur in a-SEP [24, 33]. Moreover, the thermal decomposition of intercalated NO_3^- and the dehydroxylation of the LDH laminate produces metal oxide, indicating that the structure of LDH has been destroyed [34]. Compared with PAMA, mixed powder doesn't exhibit the fourth mass-losing stage and the overall thermal decomposition rate decreases significantly, indicating that the thermal stability of PAMA can be improved by introducing a-SEP@LDH. The residual weights of PAMA, a-SEP@LDH and mixture are 24.9%, 80.4% and 51.8% at 800°C, respectively, indicating that a-SEP@LDH has outstanding heat resistance. It is worth noting that the experimental value of residual char of mixture is higher than the theoretical value, suggesting that there exists an obvious synergistic charring effect between a-SEP@LDH and PAMA.

Table 1
The TG and DTG data of PAMA, a-SEP@LDH, a-SEP@LDH-PAMA in N_2

Samples	$T_{5\%}$/℃	T_{max}/℃	Residues at 800℃/wt%	
			Experimental	Calculated
PAMA	99.6	390.0	24.9	—
a-SEP@LDH	162.6	303.1	80.4	—
a-SEP@LDH-PAMA	136.5	392.5	51.8	43.4

3.2 Dispersion of a-SEP@LDH/PAMA in EP matrix

To systematically analyze the dispersion state of flame retardants in EP matrix, the cryo-fracture cross-section of EP composites were directly observed by SEM. The roughness of the fracture cross-section reflects the interfacial interaction and dispersity between fillers and polymer matrix. As shown in Fig. 5, EP exhibits a smooth surface morphology with minimal tilted ripples due to the brittle fracture. In contrast, the fracture surfaces of EP composites become rougher and the folds increase, because PAMA or a-SEP@LDH may play a role as an impenetrable obstacle leading to crack bending and blocking [35]. Due to the existence of organic groups in PAMA and abundant hydroxyl groups in a-SEP@LDH, both EP/PAMA and EP/a-SEP@LDH have relatively good compatibility [36]. However, there are still some tiny aggregates on the cross-section (shown by arrows), which are caused by the uneven dispersion of PAMA or a-SEP@LDH in EP. The folds of EP/a-SEP@LDH are a little narrower than those of EP/PAMA, this difference is mainly ascribed to the smaller aggregate size of 1D nanofibers than 2D nanosheets. For EP/PAMA/a-SEP@LDH system, the fracture surface has no obvious agglomeration, furthermore, many

narrow folds are found, indicating the stronger interfacial interaction and excellent dispersion of PAMA and a-SEP@LDH, which is further demonstrated by the element-mapping of P, Si, Ni and Fe.

The XRD patterns of EP, EP/PAMA, EP/a-SEP@LDH and EP/a-SEP@LDH/PAMA are shown in Fig. 6, all samples appear a broad diffraction peak at around 2θ = 18°, which is the characteristic peak of amorphous structure of EP [37]. The peak at 2θ = 27.57°caused by the π-π stacking is greatly weakened in EP/PAMA, it can be caused by the reaction of the excessive -NH_2 group of PAMA with the epoxy group and the low content of PAMA. The typical peaks of (003) and (006) belonging to LDH disappear in EP/a-SEP@LDH due to the weakened van der Waals force among LDH laminates by the electrostatic interaction between a-SEP and LDH, as a result, the interlayers of LDH can be easily exfoliated [12]. Surprisingly, there is no obvious characteristic peak in EP/a-SEP@LDH/PAMA system, illustrating a satisfactory dispersion state of PAMA and a-SEP@LDH in EP matrix.

3.3 Thermal properties analysis of EP and its composites

In order to investigate the thermal properties of various samples, the glass transition temperature (T_g) was examined by means of DSC tests as shown in Fig. 7. The T_g of EP is 152.51°C, and the T_g of EP/a-SEP@LDH is slightly higher that of EP, which is attributed to the combined effects of the following two reasons: one is the charge transfer between a-SEP and LDH weakens the catalytic ring-opening effect of the Lewis acidic sites produced by inorganic nanofiller [38], the other is a-SEP@LDH can act as a physical crosslinking point at high temperature, increasing the degree of cross-linking to a certain extent [39]. It is worth to note that the T_g of EP/PAMA increases significantly to 166.39°C, the underlying reason is that the cross-linking reaction between the surplus amino of PAMA and epoxy groups, and then improves the cross-linking density. Consequently, the increased cross-linking density and the high stiffness of 2D nanosheets PAMA will restrict the mobility of molecular chains of EP [40, 41]. For EP/a-SEP@LDH/PAMA, its T_g is 9.66°C higher than that of EP/a-SEP@LDH, which is the result of the coupling action of physical crosslinking of a-SEP@LDH and chemical crosslinking of PAMA, indicating that the rigidity of the molecular chain of EP can be enhanced by introducing PAMA.

The TG and DTG curves of EP and its composites are shown in Fig. 8, and the corresponding data are listed in Table 2. There is only a single degradation stage ranging from 300°C to 500°C, and the temperature of maximum mass loss rate (T_{max}) is 385.1°C for EP. Compared to EP, the EP/PAMA, EP/a-SEP@LDH and EP/a-SEP@LDH/PAMA exhibit a reduction at a temperature of 5% mass loss ($T_{5\%}$), which is probably related to the earlier thermal decomposition of additives themselves, and promoting the premature thermal degradation of EP by the catalyzing effect of flame retardants [42]. It is worth noted that the $T_{5\%}$ value of EP/a-SEP@LDH/PAMA is lower than that of EP/a-SEP@LDH, while the T_{max} value is higher than that of EP/a-SEP@LDH, which is due to the fact that PAMA is earlier to decompose prior to a-SEP@LDH. Afterwards, the polyphosphoric acid and metaphosphoric acid formed by the thermal decomposition of PAMA will catalyze dehydration and carbonization of EP [43]. Thus, the early thermal decomposition of PAMA is helpful for EP/a-SEP@LDH/PAMA to form a protective char layer, resulting in the highest final char residues among all EP composites at 800°C. It is more noteworthy that the actual

char yield of EP/a-SEP@LDH/PAMA is 65% higher than the theoretical value, which further verifies the synergistic charring effect existing between a-SEP@LDH and PAMA.

The IPDT (Integral procedural decomposition temperature) proposed by Doyle is a thermal stability parameter of the sample, which is widely used to evaluate the intrinsic overall thermal stability of polymer materials during pyrolysis [44, 45]. The IPDT value is calculated with the following equations:

$$IPDT(℃) = A^* \bullet K^* \bullet (T_f - T_i) + T_i \quad (1)$$

$$A^* = (S_1 + S_2) / (S_1 + S_2 + S_3) \quad (2)$$

$$K^* = (S_1 + S_2) / S_1 \quad (3)$$

where A^* is the area ratio of the total experimental curve divide by the TG thermogram (S_1, S_2 and S_3 are shown in the colors of the parts of the insert), K^* is the coefficient of A^*, T_f is the final experimental temperature (800 °C), T_i is the initial experimental temperature (30 °C). The high IPDT value means the potential application of EP in high thermal resistance coatings and thermal insulation materials, and the IPDT value of EP/a-SEP@LDH/PAMA is maximum among all samples, indicating that it has the best thermal stability. Consequently, the co-catalytic degradation and charring functions of PAMA and a-SEP@LDH are responsible for these results.

Table 2
Thermal analysis data of EP and its composites in N_2

Samples	$T_{5\%}$/°C	T_{max}/°C	Residues at 800°C/wt%		IPDT/°C
			Experimental	Calculated	
EP	355.3	385.1	13.4	—	597.6
EP/PAMA	322.9	382.5	19.6	13.7	691.4
EP/a-SEP@LDH	345.3	367.7	22.3	15.4	756.4
EP/a-SEP@LDH/PAMA	338.9	387.5	23.6	14.3	787.6

3.4 Fire-retardant behavior of EP and its composites

The fire-retardancy of EP and its composites are analyzed by UL-94, LOI and CCT. The results of UL-94 test are shown in Table 3. The EP is easily ignited. In the case of 3wt% total loading of flame retardants, the EP/a-SEP@LDH passes UL-94 V-1 rating, which is due to the barrier effect and catalytic charring effect of a-SEP@LDH to delay combustion until termination. However, there is no fire rating achieved in the UL-94 test for EP/PAMA composites, because PAMA itself cannot help to produce enough stable char layer to protect internal EP matrix, and the weak blowing out effect produced by melamine is unable to kill the flame (Fig. 9). In contrast, under the dual fire-retardant action of condensed phase and gas phase, the

best fire retardancy of EP can be obtained when the mass ratio of a-SEP@LDH to PAMA is 1:2 or 1:3 at a total loading of 3wt%, which can pass UL-94 V-0 rating with self-extinguishing behavior, and the total combustion time is the shortest at the ratio of 1:2. However, when the proportion of a-SEP@LDH to PAMA is too high or too low, no satisfactory results can be achieved. Moreover, the EP composites cannot pass UL-94 V-0 rating when the total addition amount is slightly increased or decreased. The above results demonstrate that there is an optimal proportion of a-SEP@LDH to PAMA to bring about best fire retardancy for EP. The improved fire retardancy takes into account the good synergistic effect of a-SEP@LDH and PAMA, which helps to form a continuous dense char layer within a short period, so that the spread of flame is suppressed effectively. Compared with other reported work of flame retardant EP with single-component or multi-component nanomaterials (Fig. 10 and Table 4) [46–55], this work really achieves UL-94 V-0 rating at lowest addition amount by adding multi-component green flame retardant in EP. According to Fig. 11, the LOI value of EP is 26.3%. Loading flame retardants can improve the LOI values of various EP composites to varying degrees. It is worth mentioning that the EP/a-SEP@LDH/PAMA has the highest LOI value. Based on the aforementioned findings, it is concluded that a-SEP@LDH and PAMA possess a great synergistic flame retardant effect in EP.

Table 3
The results of EP/a-SEP@LDH/PAMA with different proportions in UL-94 tests

Samples	E44 monomers (wt%)	a-SEP@LDH (wt%)	PAMA (wt%)	UL-94 test		Dripping	Ratings
				av-t_1/s	av-t_2/s		
EP	100	0	0	> 30	_[a]	No	NR[b]
EP/PAMA	97	0	3	> 30	_[a]	No	NR[b]
EP/a-SEP@LDH	97	3	0	10.3	14	No	V-1
EP/a-SEP@LDH/PAMA1	97	2	1	> 30	_[a]	No	NR[b]
EP/a-SEP@LDH/PAMA2	97	1.5	1.5	13	1	No	NR[b]
EP/a-SEP@LDH/PAMA3	97	1	2	6	2	No	V-0
EP/a-SEP@LDH/PAMA4	97	0.75	2.25	5	4	No	V-0
EP/a-SEP@LDH/PAMA5	97	0.6	2.4	17	9	No	V-1
EP/a-SEP@LDH/PAMA6	97	0.5	2.5	> 30	_[a]	No	NR[b]
EP/a-SEP@LDH/PAMA7	98	0.67	1.33	6	5	No	V-1
EP/a-SEP@LDH/PAMA8	96	1.33	2.67	15	21	No	NR[b]

[a] No recorded

[b] No rating

Table 4
Comparison with the previously reported work in UL-94 test

matrix	FR additives	additive amount	UL-94	Refs
EP	MLBCN	5wt%	NR	[44]
EP	LDH-CD-Ferr	6wt%	V-1	[45]
EP	LDH-DBS@silica-1	3wt%	V-1	[46]
EP	PZMA@APP	10wt%	V-0	[47]
EP	PHDT@FeCo-LDH	4wt%	V-0	[48]
EP	MOF@GO/IFR	10wt% (0.5:9.5)	V-1	[49]
EP	CEMP/OMMT	18wt% (15:3)	V-0	[50]
EP	EG/1PANI@Fe_2O_3	8wt% (7:1)	V-0	[51]
EP	APP/T-CHS	6wt% (5.9:1)	V-0	[52]
EP	CoZn-ZIF@SCFs/APP	5 wt% (1:4)	V-0	[53]
EP	a-SEP@LDH/PAMA	3wt% (1:2)	V-0	This work

The cone calorimeter tests (CCT) can be used to evaluate the comprehensive combustion performance of polymeric materials. The time to ignition (TTI), the peak of heat release rate (pHRR), total heat release rate (THR), the peak of smoke release rate (pSPR), total CO production, total CO_2 production, and average effective heat combustion (av-EHC) are summarized in Table 5. The curves of heat release rate (HRR), smoke release rate (SPR), CO production (COP), CO_2 production (CO_2P) are shown in Fig. 12.

The TTI values of EP composites are all shorter than that of EP, implying that the initial thermal decomposition of EP is accelerated by flame retardants, which is consistent with the results of TG. The pHRR of EP is 952.6 kW/m^2, while the pHRR values of EP/PAMA and EP/a-SEP@LDH decrease to 581.5 kW/m^2 and 797.8 kW/m^2, respectively. The EP/PAMA exbibits better heat suppression effect than EP/a-SEP@LDH, which is mainly due to the expanded char layer formed by the thermal decomposition of PAMA [56]. Whereas, a-SEP@LDH alone cannot produce a good char layer under continuous heat irradiation to protect the underlying EP matrix. Compared with EP/a-SEP@LDH, the pHRR of EP/a-SEP@LDH/PAMA is decreased by 28.8% and the THR is dropped to 96MJ/m^2, representing a synergistic fire retardancy existed between a-SEP@LDH and PAMA in the combustion process, thereby resulting in an effectively protective char residue to block the transmission of heat and combustible volatiles. The av-EHC reflects the combustion of flammable volatile in the gaseous phase. The av-EHC of EP/a-SEP@LDH/PAMA is only 17.18 MJ/kg, indicating a lower heat generation in volatile gases, which can be explained by the isolation effect of high-quality char layer and the dilution effect of non-flammable gases.

The SPR reflects the parameters of smoke release in real fire. The pSPR of all EP composites is lower than that of EP. The pSPR of EP/a-SEP@LDH is larger than that of EP/PAMA, the related reason is the same as the pHRR date, that is the a-SEP@LDH is unable to promote the formation of continuous char layer, resulting in the overflow of thermal degraded fragments of EP. In contrast, PAMA itself acts as a good charring agent and the polyphosphoric acid and metaphosphoric acid generated by PAMA can catalyze the dehydration and carbonization of EP to form a swollen char layer [57]. The pSPR of EP/a-SEP@LDH/PAMA is the consequence by the joint action of a-SEP@LDH and PAMA. During the process of combustion, the pyrolytic products (polyphosphoric acid and metaphosphoric acid) formed by PAMA and degradative substances (metal compounds and various acid active sites) generated by a-SEP@LDH lead to the formation of continuous and dense char residues [58], so that more decomposition debris of EP composites adhere to it [59], and the char residue yield of EP/a-SEP@LDH/PAMA is the highest.

To study the toxicity of combustion products, the COP and CO_2P curves shown in Fig. 12(c,d), which are similar to the HRR curves. It is noteworthy that the total COP of EP/PAMA is higher than that of EP/a-SEP@LDH, while the total CO_2P is lower than that of EP/a-SEP@LDH, indicating more incomplete combustion of EP/PAMA due to more protective char layer [60]. Besides, the metal oxides originated from a-SEP@LDH can be reduced by CO to generate Ni, Fe and CO_2 during combustion. The total COP of EP/a-SEP@LDH/PAMA is between EP/PAMA and EP/a-SEP@LDH, which is the result of combined actions of incomplete combustion and redox reaction of some metal oxides during combustion. With the formation of the densest continuous carbon layer, which effectively inhibits the further oxidation of CO to CO_2 by oxygen, so the total CO_2P of EP/a-SEP@LDH/PAMA is the lowest.

Table 5
Cone calorimetric data of EP and its composites

Samples	TTI (s)	pHRR (kW/m^2)	THR (MJ/m^2)	pSPR (m^2/s)	Total COP (g)	Total CO_2P (g)	av-EHC (MJ/kg)	Char residue (wt%)
EP	96 ± 5	952.6 ± 18.9	112.8 ± 1.5	0.493 ± 0.002	3.05 ± 0.02	71.08 ± 0.97	22.77 ± 0.32	11.4 ± 1.6
EP/PAMA	95 ± 4	581.5 ± 79.7	109.9 ± 8.0	0.317 ± 0.010	3.06 ± 0.06	63.85 ± 1.93	22.69 ± 0.85	19.7 ± 1.2
EP/a-SEP@LDH	93 ± 1	797.8 ± 0.3	106.9 ± 1.7	0.430 ± 0.025	2.68 ± 0.06	69.41 ± 0.99	21.12 ± 0.07	17.1 ± 2.0
EP/a-SEP@LDH/PAMA	89 ± 3	568.1 ± 15.7	96.0 ± 0.7	0.345 ± 0.020	2.74 ± 0.07	60.70 ± 0.18	17.18 ± 2.70	19.9 ± 1.2

3.5 Fire retardant mechanism

In order to elucidate the fire retardant mechanism, SEM, Raman, XRD and FTIR were adopted to characterize the char residues of EP and its composites obtained from CCT. As shown in Fig. 13a, there are only a few discontinuous char residues for EP, and obvious cracks (marked with the orange arrow) in the interior char residue for EP. Compared with EP, the thickness of the char residues of EP composites is greatly increased. The continuous residual char of EP/PAMA can be observed, but there are many holes on top, resulting in a loose expanded char layer. However, its internal char layer is dense and continuous, which can relatively inhibit the transfer of oxygen and heat. Concerning EP/a-SEP@LDH, the external residual char exhibits visible defects, while the interior char contains a few broken bubbles and serried weeny metal oxide particles formed by the thermal decomposition of a-SEP@LDH. After combining PAMA and a-SEP@LDH, the whole char layer is quite compact and continuous. The co-catalytic carbonization of PAMA and a-SEP@LDH, as well as the physical reinforcement of sepiolite nanofibers, are thought to generate a high-quality char layer, which can effectively prevent the overflow of thermal degradation debris.

Raman spectroscopy is commonly used to analyze the graphitization degree of char residue. As shown in Fig. 14, each figure exhibits one broad peaks at 1367cm^{-1} and one sharp peak at 1597cm^{-1}, corresponding to D and G bands, respectively. In general, the D bands represent the disordered graphite or glassy carbon, and the G bands correspond to absorption peak of the sp^2-hybridized carbon atoms. The integral strength ratio of D to G bands correlates to the graphitization degree of residual char. Lower values of I_D/I_G represent higher degree of graphitization [61]. As seen, the I_D/I_G value of EP/a-SEP@LDH is 1.66, whereas the I_D/I_G of EP/a-SEP@LDH/PAMA is lowest among the other control groups. These results illustrate that the cooperative catalyzing charring effects from PAMA and a-SEP@LDH can produce more graphitization structure, which can serve to a high-quality char layer and block the transfer of heat and gases essentially.

To further analyze the phase composition, the char residue formed in CCT tests are analyzed by XRD. As shown in Fig. 15, There is a broad diffraction peak around 25° for both EP and EP/a-SEP@LDH/PAMA, corresponding to the (002) diffraction peak of graphite. In addition, for EP/a-SEP@LDH/PAMA, it shows a characteristic diffraction peak at 7.3°, which is ascribed to the sepiolite fiber structure [62]. This finding identifies that the fiber structure of sepiolite is preserved in residual char owing to its high thermal stability, and then this fiber structure physically reinforces the protective char layer during combustion. There also exists Ni,Fe alloys (PDF#12–0736), NiO (PDF#78–0423) and Fe_3O_4 (PDF#76-1849), because Fe^{3+}, Ni^{2+} can undergo redox reactions with the thermal degradation products of EP such as CO ($Fe^{3+}\rightarrow Fe^{2+}\rightarrow Fe$, $Ni^{2+}\rightarrow Ni$, $CO\rightarrow CO_2$) [12]. These metal oxides generated during thermal decomposition have a high specific heat capacity, which will contribute to excellent heat absorption [63]. Meanwhile, Sepiolite may produce a large number of Brønsted acidic sites, Fe^{3+} and Ni^{2+} can act as Lewis acidic sites under high temperature, and all these acidic sites may attack EP molecular chains to generate cationic active sites, thereby accelerating and catalyzing the pyrolysis, isomerization and aromatization

reaction of polymer [64–66], consequently promoting the formation of stable and continuous thick coke layer.

To further illustrate the role of PAMA, the FTIR spectra of char residue from EP and EP/a-SEP@LDH/PAMA are given in Fig. 16. The characteristic peak at 3431cm^{-1} is attributed to O-H or N-H stretching vibration, the peaks at 2923cm^{-1} and 2832cm^{-1} are caused by -CH_2- and -CH-, respectively [67]. The absorption peak at 1589cm^{-1} is assigned to phenyl [68] and the peak at 1105cm^{-1} belong to C-O bond in ether group [69]. Additionally, for EP/a-SEP@LDH/PAMA, the characteristic peaks at 1234cm^{-1} and 1178cm^{-1} are attributed to P = O and P-O groups, respectively [70]. The peak at 1121cm^{-1} can be ascribed to the stretching vibration of PO_2/PO_3 in phosphate carbon complexes [71]. These results demonstrating that PAMA can form polyphosphoric acid and phosphoric acid, which has an excellent dehydration and carbonization effect during combustion. The weak absorption peak at 951cm^{-1} and 457cm^{-1} belong to Si-O-Si bond of a-SEP. The stretching vibration peak of Fe-O and the bending vibration peak of Ni-O occur at 561cm^{-1} and 608cm^{-1} [72, 73], respectively. These further prove that the a-SEP can act as physical reinforcement for the char layer and metal oxides exist in the residue. Compared to EP, a new vibrational peak appeared at 1509cm^{-1} in EP/a-SEP@LDH/PAMA is originated from the aromatic ring [74], indicating that the formed char layer has a higher degree of aromatization, thereby effectively improving the fireproofing properties.

Based on the foregoing discussion, the possible synergistic fire retardant mechanism of PAMA and a-SEP@LDH in EP may be proposed, as showed in Scheme 2. In the combustion process of the EP/a-SEP@LDH/PAMA system, on the one hand, PAMA can thermally decompose to produce polyphosphoric acid and phosphoric acid, which promote the dehydration and carbonization of EP molecular chain, and then forms an expanded char layer. Besides, the carbonaceous PAMA nanosheets may function as a solid physical barrier and offer strong smoke suppression properties. On the other hand, the metal oxides generated by a-SEP@LDH can effectively absorb heat. In addition, the varieties of acidic sites will accelerate the pyrolysis, isomerization and aromatization reactions of EP, facilitating to obtain efficient protective char layer with a high graphitization structure. Meanwhile, sepiolite fiber, as a kind of inorganic nano-clay with strong thermal stability, can physically strengthen the char layer and considerably improve the thermostability of char residue. As a result, the formed high-quality and high-stability char layer can effectively inhibit the transfer of oxygen and heat between combustible zone and the matrix. Moreover, the release of smoke and volatiles is also suppressed, and the amount of char residue increases noticeably.

3.6 Mechanical properties of EP and its composites

The tensile strength and impact strength are used to analyze the mechanical properties of EP and EP composites. The corresponding results are shown in Fig. 17 and Table 6. In our previous work [12], the tensile strength of EP/a-SEP@LDH with 2.3wt% loading is 21.57% higher than that of pure EP, but when the addition of a-SEP@LDH is 3wt%, the tensile strength is only slightly increased by 5.46% compared to EP, which may be caused by the partial agglomeration of a-SEP@LDH in EP matrix (as shown in Fig. 5c).

However, when PAMA is added to system, the tensile and impact strengths of EP/a-SEP@LDH/PAMA are 33.8% and 42.8% higher than those of EP, respectively. Meanwhile, an increased Young Modulus is also obtained. These marked improvements imply an excellent synergy between PAMA and a-SEP@LDH. The following are some possible explanations: a) as discussed in section 3.3, the physical crosslinking of a-SEP@LDH and chemical crosslinking of PAMA make for improving the cross-linking density, coupled with the “circuitous effect” of nanofillers [75], limits the mobility of EP molecular segments to a certain extent. b) the increased dispersion of EP/a-SEP@LDH/PAMA is beneficial to enhance the interfacial interaction between the nanofillers and EP matrix, thereby allowing stress to be rapidly transferred from the weak polymer interfaces to tough nanolayers or nanofibers when subjected to external force. c) more wrinkles and surface roughness on the cross-section of EP/a-SEP@LDH/PAMA, indicate that the combination of PAMA and a-SEP@LDH can boost fracture energy dissipation (in Fig. 5d).

Table 6
The mechanical properties of EP and its composites

Samples	Impact strength (KJ/m^2)	Tensile strength (MPa)	Elongation at break (%)	Young Modulus (GPa)
EP	10.61 ± 1.30	57.90 ± 1.91	6.18 ± 0.48	1.22 ± 0.02
EP/PAMA	13.76 ± 0.65	66.03 ± 4.98	5.82 ± 0.35	1.63 ± 0.02
EP/a-SEP@LDH	7.62 ± 0.11	61.06 ± 3.80	4.72 ± 0.30	1.69 ± 0.03
EP/a-SEP@LDH/PAMA	15.15 ± 0.19	77.49 ± 3.54	5.79 ± 0.42	1.73 ± 0.02

4 Conclusions

The phytic-based P/N-containing nanosheet (PAMA) was employed to improve the flame retardant efficiency of inorganic hybrid nanofiber (a-SEP@LDH) in EP. By adding only 1wt% a-SEP@LDH and 2wt% PAMA to EP, the UL-94 V-0 rating and the LOI value of 31.6% are reached. The EP/a-SEP@LDH/PAMA has a stronger thermal stability than EP, and its IPDT value is enhanced by 31.8%. Additionally, the pHRR and pSPR of EP/a-SEP@LDH/PAMA are greatly reduced. The fire retardant mechanism of EP/a-SEP@LDH/PAMA mostly depends on condensed phase behavior. During burning, polyphosphoric acid and phosphoric acid, metal oxides and various acidic sites can catalyze the cross-linking, aromatization and carbonization of EP, combining with the strengthening effect of a-SEP fiber to produce a more stable, continuous and solidary char layer. What`s more, the synergistic actions of a-SEP@LDH and PAMA lead to improved dispersion and fracture energy dissipation, which are beneficial to reinforce the mechanical properties of EP. Thereby, the impact strength and tensile strength of EP/a-SEP@LDH/PAMA are 42.8% and 33.8% higher, respectively, than those of EP. In short, our study really achieves excellent fire retardancy with a minimum addition amount of flame retardant in EP, along with improved mechanical properties without compromising heat resistance.

Declarations

Funding This work was financially supported by the National Natural Science Foundation of China (No. 51973178; 51673160), and Supported by the Open Project Program (BTBUFR22-2) of China Light Industry Engineering Technology Research Center of Advanced Flame Retardants, Beijing Technology and Business University, China.

Conflict of interest: the authors declare no competing interests.

Author's contribution:

Suhua Zhang: Investigation, Date processing, Writing-original draft preparation, Visualization.

Zhenzhong Wu: Methodology.

Shihu Han: Validation, Methodology.

Yiqing Wang: Conceptualization.

Lijun Qian: Funding acquisition, Writing reviewing and editing.

Xiaoping Hu: Supervision, Funding acquisition, Writing reviewing and editing.

All authors have reviewed and approved the manuscript.

References

1. Huo SQ, Song PA, Yu B, Ran SY, Chevali VS, Liu L, Fang ZP, Wang H (2021) Phosphorus-containing flame retardant epoxy thermosets: Recent advances and future perspectives. Prog Polym Sci 114:101366. https://doi.org/10.1016/j.progpolymsci.2021.101366
2. Chen XS, Peng FC, Wang C, Zhou HF, Lin XB, Wei L, Zhang AQ (2022) Improving the flame retardancy and mechanical properties of epoxy composites significantly with a low-loading CNT-based hierarchical hybrid decorated with reactive hyperbranched polyphosphoramide. Appl Surf Sci 576:151765. https://doi.org/10.1016/j.apsusc.2021.151765
3. Liu C, Li P, Xu YJ, Liu Y, Zhu P, Wang YZ (2022) Epoxy/iron alginate composites with improved fire resistance, smoke suppression and mechanical properties. J Mater Sci 57:2567-2583. https://doi.org/10.1007/s10853-021-06671-x
4. Huo SQ, Wang J, Yang S, Li C, Wang XL, Cai HP (2019) Synthesis of a DOPO-containing imidazole curing agent and its application in reactive flame retarded epoxy resin. Polym Degrad Stab 159:79-89. https://doi.org/10.1016/j.polymdegradstab.2018.11.021
5. Zhang QQ, Wang J, Yang S, Cheng JW, Ding GP, Hu YF, Huo SQ (2020) Synthesis of a P/N/S-based flame retardant and its flame retardant effect on epoxy resin. Fire Saf J 113:102994.

6. Chen YS, Duan HJ, Ji S, Ma HR (2021) Novel phosphorus/nitrogen/boron-containing carboxylic acid as co-curing agent for fire safety of epoxy resin with enhanced mechanical properties. J Hazard Mater 402:123769. https://doi.org/10.1016/j.jhazmat.2020.123769
7. Zhang JH, Kong QH, Wang DY (2018) Simultaneously improving the fire safety and mechanical properties of epoxy resin with Fe-CNTs via large-scale preparation. J Mater Chem A 6:6376-6386. https://doi.org/10.1039/C7TA10961J
8. Ai YF, Pang FQ, Xu YL, Jian RK (2020) Multifunctional Phosphorus-Containing Triazolyl Amine toward Self-Intumescent Flame-Retardant and Mechanically Strong Epoxy Resin with High Transparency. Ind Eng Chem Res 59:11918-11929. https://doi.org/10.1021/acs.iecr.0c01277
9. Wu HY, Zeng BR, Chen JM, Wu T, Li YT, LiuYZ, Dai LZ (2019) An intramolecular hybrid of metal polyhedral oligomeric silsesquioxanes with special titanium-embedded cage structure and flame retardant functionality. Chem Eng J 374:1304-1316. https://doi.org/10.1016/j.cej.2019.06.027
10. Meng WH, Wu HJ, Bi X, Huo ZY, Wu JN, Jiao YH, Xu JZ, Wang M, Qu HQ (2021) Synthesis of ZIF-8 with encapsulated hexachlorocyclotriphosphazene and its quenching mechanism for flame-retardant epoxy resin. Micropor Mesopor Mat 314:110885. https://doi.org/10.1016/j.micromeso.2021.110885
11. Liu LB, Xu Y, Xu MJ, Li ZQ, Hu YM, Li B (2019) Economical and facile synthesis of a highly efficient flame retardant for simultaneous improvement of fire retardancy, smoke suppression and moisture resistance of epoxy resins. Compos B Eng 167:422-433. https://doi.org/10.1016/j.compositesb.2019.03.017
12. Zhang HJ, Hu XP, Liu YR, Zhang SH, Wu ZZ (2021) Convenient synthesis of one-dimensional a-SEP@LDH via self-assembly towards simultaneously improved fire retardance, mechanical strength and thermal resistance for epoxy resin. Compos B Eng 216:108857. https://doi.org/10.1016/j.compositesb.2021.108857
13. Shen D, Xu YJ, Long JW, Shi XH, Chen L, Wang YZ (2017) Epoxy resin flame-retarded via a novel melamine-organophosphinic acid salt: Thermal stability, flame retardance and pyrolysis behavior. J Anal Appl Pyrol 128:54-63. https://doi.org/10.1016/j.jaap.2017.10.025
14. Wang PJ, Liao DJ, Hu XP, Pan N, Li WX, Wang DY, Yao Y (2019) Facile fabrication of biobased P-N-C-containing nano-layered hybrid: preparation, growth mechanism and its efficient fire retardancy in epoxy. Polym Degrad Stab 159:153-162. https://doi.org/10.1016/j.polymdegradstab.2018.11.024
15. Qin PF, Yi DQ, Hao JW, Ye XM, Gao M, Song TL (2021) Fabrication of melamine trimetaphosphate 2D supermolecule and its superior performance on flame retardancy, mechanical and dielectric properties of epoxy resin. Compos B Eng 225:109269. https://doi.org/10.1016/j.compositesb.2021.109269
16. Rao WH, Hu ZY, Xu HX, Xu YJ, Qi M, Liao W, Xu SM, Wang YZ (2017) Flame-retardant flexible polyurethane foams with highly efficient melamine salt. Ind Eng Chem Res 56:7112-7119. https://doi.org/10.1021/acs.iecr.7b01335
17. Mircescu NE, Oltean M, Chiş V, Leopold N, FTIR (2012) FT-Raman, SERS and DFT study on melamine. Vib Spectrosc 62:165-171. https://doi.org/10.1016/j.vibspec.2012.04.008

18. Huang ST, Wang GL, Li NB, Luo HQ (2012) Mechanism of the pH-induced aggregation reaction between melamine and phosphate. RSC Adv 2:10948-10954. https://doi.org/10.1039/C2RA21415F
19. Zhang JT, Qu LT, Shi GQ, Liu JY, Chen JF, Dai LM (2016) N, P-codoped carbon networks as efficient metal-free bifunctional catalysts for oxygen reduction and hydrogen evolution reactions. Angew Chem 128:2270-2274. https://doi.org/10.1002/ange.201510495
20. Li WX, Zhang HJ, Hu XP, Yang WX, Cheng Z, Xie CQ (2020) Highly efficient replacement of traditional intumescent flame retardants in polypropylene by manganese ions doped melamine phytate nanosheets. J Hazard Mater 398:123001. https://doi.org/10.1016/j.jhazmat.2020.123001
21. Zhang T, Yan HQ, Shen L, Fang ZP, Zhang XM, Wang JJ, Zhang BY (2014) Chitosan/phytic acid polyelectrolyte complex: a green and renewable intumescent flame retardant system for ethylene–vinyl acetate copolymer. Ind Eng Chem Res 53:19199-19207. https://doi.org/10.1021/ie503421f
22. Perraki T, Orfanoudaki A (2008) Study of raw and thermally treated sepiolite from the Mantoudi area, Euboea, Greece. J Therm Anal Calorim 91:589-593. https://doi.org/10.1007/s10973-007-8329-8
23. Li AJ, Xu WZ, Chen R, Liu YC, Li W (2018) Fabrication of zeolitic imidazolate frameworks on layered double hydroxide nanosheets to improve the fire safety of epoxy resin. Compos A Appl Sci Manuf 112:558-571. https://doi.org/10.1016/j.compositesa.2018.07.001
24. Chang Y, Liu ZH, Fu ZB, Wang CY, Dai YT, Peng RF, Hu XP (2014) Preparation and characterization of one-dimensional core–shell sepiolite/polypyrrole nanocomposites and effect of organic modification on the electrochemical properties. Ind Eng Chem Res 53:38-47. https://doi.org/10.1021/ie402226z
25. Nayak S, Mohapatra L, Parida K (2015) Visible light-driven novel g-C_3N_4/NiFe-LDH composite photocatalyst with enhanced photocatalytic activity towards water oxidation and reduction reaction. J Mater Chem A 3:18622-18635. https://doi.org/10.1039/C5TA05002B
26. Ghonchepour E, Islami MR, Bananezhad B, Mostafavi H, Tikdari AM (2019) Synthesis of recoverable palladium composite as an efficient catalyst for the reduction of nitroarene compounds and Suzuki cross-coupling reactions using sepiolite clay and magnetic nanoparticles (Fe_3O_4@sepiolite-Pd^{2+}). Comptes Rendus Chimie 22:84-95. https://doi.org/10.1016/j.crci.2018.07.008
27. Peng HY, Wang D, Li M, Zhang LP, Liu MM, Fu SH (2019) N-P-Zn-containing 2D supermolecular networks grown on MoS_2 nanosheets for mechanical and flame-retardant reinforcements of polyacrylonitrile fiber. Chem Eng J 372 873-885. https://doi.org/10.1016/j.cej.2019.04.209
28. Yang HC, Wang CH, Zhang YJ, Wang QB (2019) Green synthesis of NiFe LDH/Ni foam at room temperature for highly efficient electrocatalytic oxygen evolution reaction. Sci China Mater 62:681-689. https://doi.org/10.1007/s40843-018-9356-1
29. Xue XY, Yu F, Li JG, Bai G, Yuan HF, Hou J, Peng BH, Chen L, Yuen MF, Wang G, Wang F, Wang CD (2020) Polyoxometalate intercalated NiFe layered double hydroxides for advanced water oxidation. Int J Hydrogen Energy 45:1802-1809. https://doi.org/10.1016/j.ijhydene.2019.11.038
30. Camino G, Costa L, Trossarelli L (1985) Study of the mechanism of intumescence in fire retardant polymers: Part V—Mechanism of formation of gaseous products in the thermal degradation of

ammonium polyphosphate. Polym Degrad Stab 12:203-211. https://doi.org/10.1016/0141-3910(85)90089-8

31. Chen WY, Wang L, Liu G (2012) Synthesis of ammonium polyphosphate with crystalline form V (APP-V) from melamine polyphosphate (MPP). Polym Degrad Stab 97:2567-2570. https://doi.org/10.1016/j.polymdegradstab.2012.07.007
32. Wang ZZ, Lv P, Hu Y, Hu KL (2009) Thermal degradation study of intumescent flame retardants by TG and FTIR: Melamine phosphate and its mixture with pentaerythritol. J Anal Appl Pyrolysis 86:207-214. https://doi.org/10.1016/j.jaap.2009.06.007
33. Dong RF, Chen DY, Li NJ, Xu QF, Li H, He JH, Lu JM (2020) Removal of phenol from aqueous solution using acid-modified Pseudomonas putida-sepiolite/ZIF-8 bio-nanocomposites. Chemosphere 239:124708. https://doi.org/10.1016/j.chemosphere.2019.124708
34. Zhou LJ, Huang XX, Chen H, Jin PP, Li GD Zou XX (2015) High surface area flower-like Ni–Fe layered double hydroxide for electrocatalytic water oxidation reaction. Dalton Trans 44:11592-11600. https://doi.org/10.1039/C5DT01474C
35. Wei W, Cui YQ, Li XJ, Gu Y, Fei XM, Luo J, Liu XY (2019) Reactive particles from in situ silane-polycondensation-induced self-assembly of poly (styrene-alt-maleic anhydride) as toughener for epoxy resins. J Appl Polym Sci 136:47565. https://doi.org/10.1002/app.47565
36. Chen HX, Zheng MS, Sun HY, Jia QM (2007) Characterization and properties of sepiolite/polyurethane nanocomposites. Mater Sci Eng A 445:725-730. https://doi.org/10.1016/j.msea.2006.10.008
37. Wang X, Kalali EN, Wang DY (2015) Renewable cardanol-based surfactant modified layered double hydroxide as a flame retardant for epoxy resin. ACS Sustain Chem Eng 3:3281-3290. https://doi.org/10.1021/acssuschemeng.5b00871
38. Karami Z, Jouyandeh M, Ali JA, Ganjali MR, Aghazadeh M, Paran SMR, Naderi G, Puglia D, Saeb MR (2019) Epoxy/layered double hydroxide (LDH) nanocomposites: Synthesis, characterization, and Excellent cure feature of nitrate anion intercalated Zn-Al LDH. Prog Org Coat 136:105218. https://doi.org/10.1016/j.porgcoat.2019.105218
39. Zhang J, Li Z, Shao ZB, Zhang L, Wang DY (2020) Hierarchically tailored hybrids via interfacial-engineering of self-assembled UiO-66 and prussian blue analogue: Novel strategy to impart epoxy high-efficient fire retardancy and smoke suppression. Chem Eng J 400:125942. https://doi.org/10.1016/j.cej.2020.125942
40. Zhang QQ, Yang S, Wang J, Cheng JW, Zhang QX, Ding GP, Hu YF, Huo SQ (2019) A DOPO based reactive flame retardant constructed by multiple heteroaromatic groups and its application on epoxy resin: curing behavior, thermal degradation and flame retardancy. Polym Degrad Stab 167:10-20. https://doi.org/10.1016/j.polymdegradstab.2019.06.020
41. Sun ZZ, Hou YB, Hu Y, Hu WZ (2018) Effect of additive phosphorus-nitrogen containing flame retardant on char formation and flame retardancy of epoxy resin. Mater Chem Phys 214:154-164. https://doi.org/10.1016/j.matchemphys.2018.04.065

42. Kalali EN, Wang X, Wang DY (2016) Synthesis of Fe_3O_4 Nano-Sphere@MgAl Layered Double Hydroxide Hybrid and Application in Fabricating Multifunctional Epoxy Nanocomposites. Ind Eng Chem Res 55:6634-6642. https://doi.org/10.1021/acs.iecr.5b04873
43. Huang GB, Chen SQ, Song PA, Lu PP, Wu CL (2014) Combination effects of graphene and layered double hydroxides on intumescent flame-retardant poly(methyl methacrylate) nanocomposites. Appl Clay Sci 88–89:78-85. https://doi.org/10.1016/j.clay.2013.11.002
44. Doyle CD (1961) Estimating thermal stability of experimental polymers by empirical thermogravimetric analysis. Anal Chem 33:77-79. https://doi.org/10.1021/ac60169a022
45. Park SJ, Kim HC (2001) Thermal stability and toughening of epoxy resin with polysulfone resin. J Polym Sci Part B Polym Phys 39 121-128. https://doi.org/10.1002/1099-0488(20010101)39:1<121::AID-POLB110>3.0.CO;2-N
46. Wang JL, Zhou HB, Wang ZR, Bai W, Cao YF, Wei YN (2022) Constructing hierarchical structure based on LDH anchored boron-doped g-C_3N_4 assembled with MnO_2 nanosheets towards reducing toxicants generation and fire hazard of epoxy resin. Compos B Eng 229:109453. https://doi.org/10.1016/j.compositesb.2021.109453
47. Li Z, Liu ZQ, Zhang J, Fu C, Wagenknecht U, Wang DY (2019) Bio-based layered double hydroxide nanocarrier toward fire-retardant epoxy resin with efficiently improved smoke suppression. Chem Eng J 378:122046. https://doi.org/10.1016/j.cej.2019.122046
48. Li Z, Liu ZQ, Dufosse F, Yan LK, Wang DY (2018) Interfacial engineering of layered double hydroxide toward epoxy resin with improved fire safety and mechanical property. Compos B Eng 152:336-346. https://doi.org/10.1016/j.compositesb.2018.08.094
49. Qiu SL, Ma C, Wang X, Zhou X, Feng XM, Yuen RK, Hu Y (2018) Melamine-containing polyphosphazene wrapped ammonium polyphosphate: A novel multifunctional organic-inorganic hybrid flame retardant. J Hazard Mater 344:839-848. https://doi.org/10.1016/j.jhazmat.2017.11.018
50. Sui YL, Sima HF, Shao WD, Zhang CL (2022) Novel bioderived cross-linked polyphosphazene microspheres decorated with FeCo-layered double hydroxide as an all-in-one intumescent flame retardant for epoxy resin. Compos B Eng 229:109463. https://doi.org/10.1016/j.compositesb.2021.109463
51. Zhang J, Li Z, Zhang L, Molleja JG, Wang DY (2019) Bimetallic metal-organic framework and graphene oxide nano-hybrids induced carbonaceous reinforcement towards fire retardant epoxy: A novel alternative carbonization mechanism. Carbon 153:407-416. https://doi.org/10.1016/j.carbon.2019.07.003
52. Yu HH, Xu XH, Xia YF, Pan MZ, Zarshad N, Pang B, Rahman AU, Wu M, Ni HM (2020) Synthesis of a novel modified chitosan as an intumescent flame retardant for epoxy resin. e-Polymers 20:303-316. https://doi.org/10.1515/epoly-2020-0036
53. Chen ZW, Xu YY, Yu Y, Chen TT, Zhang QW, Li CX, Jiang JC (2021) Polyaniline-modified Fe_2O_3/expandable graphite: A system for promoting the flame retardancy, mechanical properties and

electrical properties of epoxy resin. Powder Tech 378:359-370. https://doi.org/10.1016/j.powtec.2020.10.002

54. Liu FY, Zhou XL, Zhao H, Hu WD, Xu JZ, Jiao YH, Qu HQ (2022) The synergistic flame retardant, smoke suppressant, and thermal degradation properties of spherical CoSn (OH) 6 and ammonium polyphosphate on epoxy resin. J Therm Anal Calorim 147:9431-9450. https://doi.org/10.1007/s10973-021-11188-1
55. Lin J, Wang KQ, Li JG, Yang DS, Zhu YY, WangXL (2021) Growing metal-organic framework nanoparticles on short carbon fibers to improve flame retardancy, smoke suppression and mechanical properties of the flame retardant epoxy composites. J Mater Sci 56:19899-19914. https://doi.org/10.1007/s10853-021-06507-8
56. Jin SL, Liu Z, Qian LJ, Qiu Y, Chen YJ, Xu B (2020) Epoxy thermoset with enhanced flame retardancy and physical-mechanical properties based on reactive phosphaphenanthrene compound. Polym Degrad Stab 172:109063. https://doi.org/10.1016/j.polymdegradstab.2019.109063
57. Yang S, Wang J, Huo SQ, Wang M, Wang JP, Zhang B (2016) Synergistic flame-retardant effect of expandable graphite and phosphorus-containing compounds for epoxy resin: Strong bonding of different carbon residues. Polym Degrad Stab 128:89-98. https://doi.org/10.1016/j.polymdegradstab.2016.03.017
58. Wei J, Yao RW, Ge QJ, Xu DY, Fang CY, Zhang JX, Xu HY, Sun J (2021) Precisely regulating Brønsted acid sites to promote the synthesis of light aromatics via CO_2 hydrogenation. Appl Catal B Environ 283:119648. https://doi.org/10.1016/j.apcatb.2020.119648
59. Ma C, Li J (2019) Synthesis of an organophosphorus flame retardant derived from daidzein and its application in epoxy resin. Compos B Eng 178:107471. https://doi.org/10.1016/j.compositesb.2019.107471
60. Jiang Q, Li P, Liu Y, Zhu P (2022) Green flame-retardant flexible polyurethane foam based on polyphenol-iron-phytic acid network to improve the fire safety. Compos B Eng 239:109958. https://doi.org/10.1016/j.compositesb.2022.109958
61. Chen ZQ, Jiang JC, Yu Y, Chen G, Chen TT, Zhang QW (2021) Layer-by-layer assembled bagasse to enhance the fire safety of epoxy resin: A renewable environmental friendly flame retardant. J Appl Polym Sci 138:50032. https://doi.org/10.1002/app.50032
62. Soheilmoghaddam M, Wahit MU, Yussuf AA, Al-Saleh MA, Whye WT (2014) Characterization of bio regenerated cellulose/sepiolite nanocomposite films prepared via ionic liquid. Polym testing 33:121-130. https://doi.org/10.1016/j.polymertesting.2013.11.011
63. Hou YB, Hu WZ, Gui Z, Hu Y (2017) Preparation of metal-organic frameworks and their application as flame retardants for polystyrene. Ind Eng Chem Res 56:2036-2045. https://doi.org/10.1021/acs.iecr.6b04920
64. Gallo E, Schartel B, Acierno D, Russo P (2011) Flame retardant biocomposites: Synergism between phosphinate and nanometric metal oxides. Eur Polym J 47:1390-1401. https://doi.org/10.1016/j.eurpolymj.2011.04.001

65. Hong J, Wu T, Wang X, Lu ZW, Zhang JL, Zeng BR, Yuan CH, Dai LZ (2022) Copper-catalyzed pyrolysis of halloysites@polyphosphazene for efficient carbonization and smoke suppression. Compos B Eng 230:109547. https://doi.org/10.1016/j.compositesb.2021.109547
66. Gong J, Chen XC, Tang T (2019) Recent progress in controlled carbonization of (waste) polymers. Prog Polym Sci 94:1-32. https://doi.org/10.1016/j.progpolymsci.2019.04.001
67. Yang WX, Zhang HJ, Hu XP, Liu YR, Zhang SH, Xie CQ (2021) Self-assembled bio-derived microporous nanosheet from phytic acid as efficient intumescent flame retardant for polylactide. Polym Degrad Stab 191:109664. https://doi.org/10.1016/j.polymdegradstab.2021.109664
68. Qi Z, Zhang WC, He XD, Yang RJ (2016) High-efficiency flame retardency of epoxy resin composites with perfect T_8 caged phosphorus containing polyhedral oligomeric silsesquioxanes (P-POSSs). Compos Sci Tech 127:8-19. https://doi.org/10.1016/j.compscitech.2016.02.026
69. Zhang PK, Fan HJ, Tian SQ, Chen Y, Yan J (2016) Synergistic effect of phosphorus-nitrogen and silicon-containing chain extenders on the mechanical properties, flame retardancy and thermal degradation behavior of waterborne polyurethane. RSC Adv 6:72409-72422. https://doi.org/10.1039/C6RA15869B
70. Li N, Ming J, Yuan RC, Fan S, Liu L, Li FX, Wang XL, Yu JY, Wu DQ (2019) Novel eco-friendly flame retardants based on nitrogen–silicone schiff base and application in cellulose. ACS Sustain Chem Eng 8:290-301. https://doi.org/10.1021/acssuschemeng.9b05338
71. Yang G, Wu WH, Wang YH, Jiao TH, Lu LY, Qu HQ, Qin XY (2019) Synthesis of a novel phosphazene-based flame retardant with active amine groups and its application in reducing the fire hazard of Epoxy Resin. J Hazard Mater 366:78-87. https://doi.org/10.1016/j.jhazmat.2018.11.093
72. Li Z, Cheng XY, Liu YJ, Liu H, Jiang Y, Wang N (2022) Intumescent flame retardancy and smoke suppression of Eucommia ulmoides gum/natural rubber blends based on synergistic g-C_3N_4@Fe_3O_4 nanocomposites. RSC Adv 12:21704-21712. https://doi.org/10.1039/D2RA03377A
73. Bao QR, Liu Y, He R, Wang Q (2021) The effect of strawberry-like nickel-decorated flame retardant for enhancing the fire safety and smoke suppression of epoxy resin. Polym Degrad Stab 193:109740. https://doi.org/10.1016/j.polymdegradstab.2021.109740
74. Yang HY, Xin W, Yu B, Lei S, Yuan H, Yuen RK (2012) Effect of borates on thermal degradation and flame retardancy of epoxy resins using polyhedral oligomeric silsesquioxane as a curing agent. Therm Acta 535:71-78. https://doi.org/10.1016/j.tca.2012.02.021
75. Fang F, Ran SY, Fang ZP, Song PA, Wang H (2019) Improved flame resistance and thermo-mechanical properties of epoxy resin nanocomposites from functionalized graphene oxide via self-assembly in water. Compos B Eng 165:406-416. https://doi.org/10.1016/j.compositesb.2019.01.086

Scheme

Scheme 1 and 2 are available in the Supplementary Files section

Figures

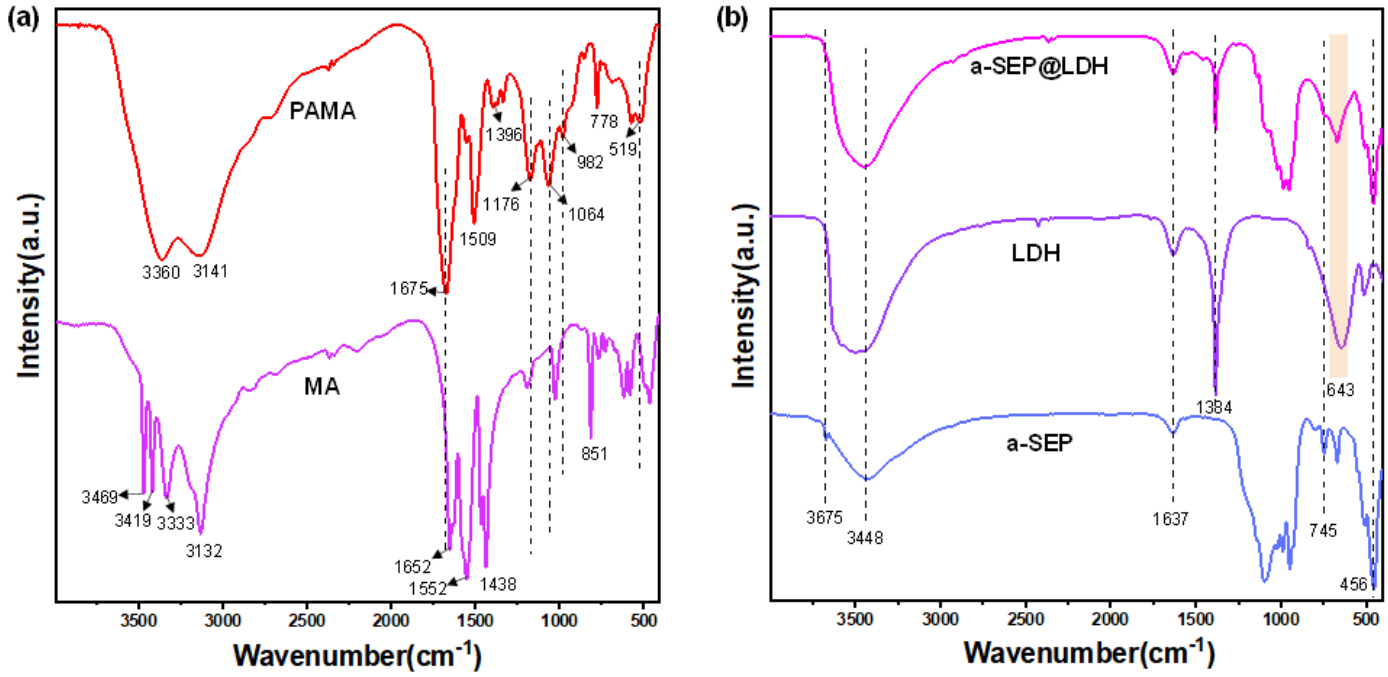


Figure 1

FTIR spectra of (a) MA, PAMA, (b) a-SEP, LDH and a-SEP@LDH

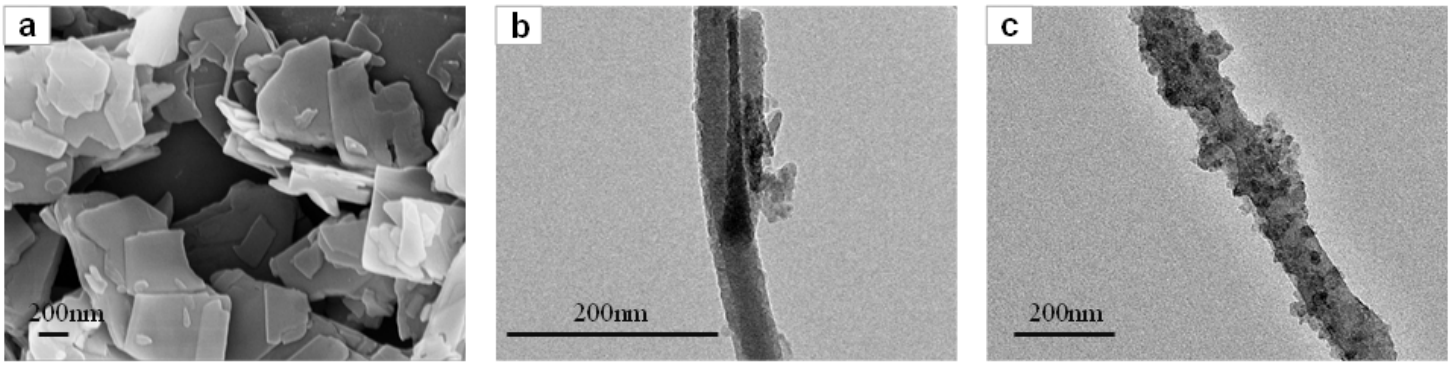


Figure 2

SEM image of PAMA(a) and TEM image of a-SEP (b) and a-SEP@LDH(c)

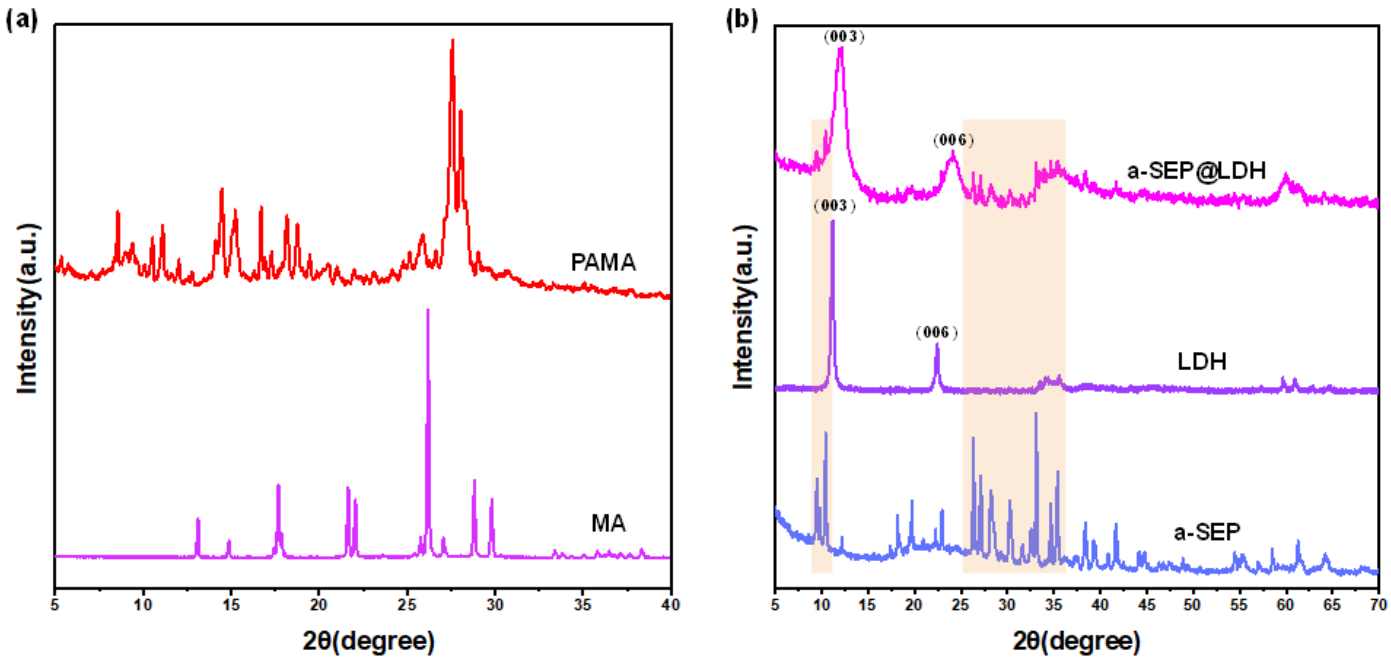


Figure 3

XRD patterns of (a)MA, PAMA, (b) a-SEP, LDH and a-SEP@LDH

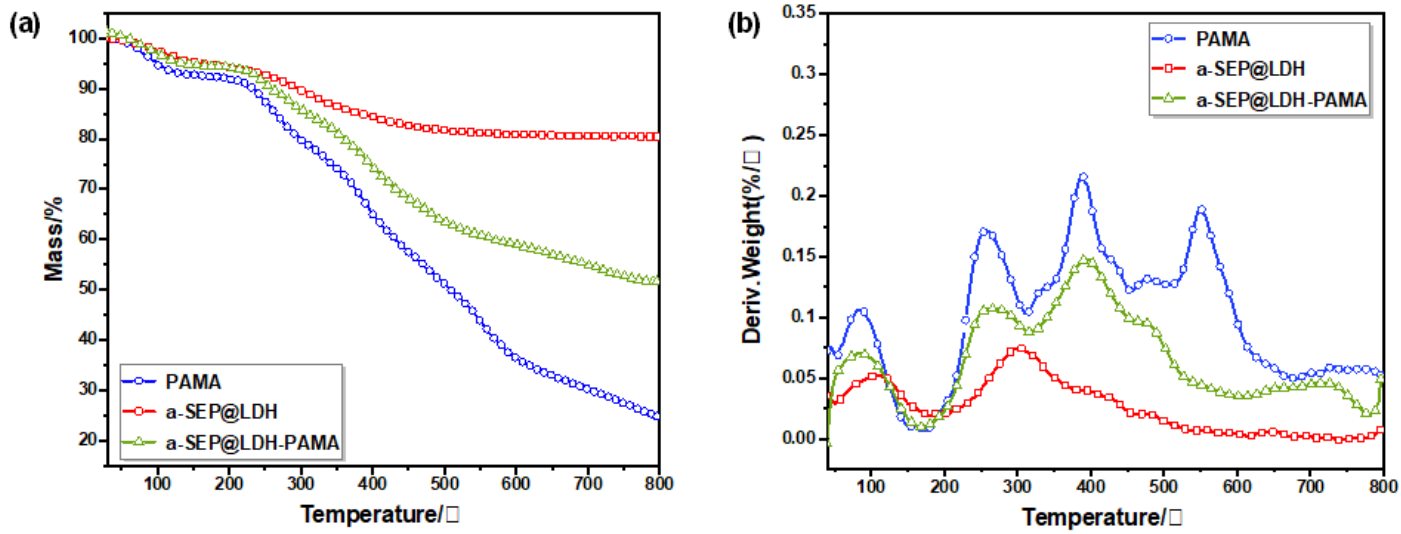


Figure 4

TG (a) and DTG (b) curves of PAMA, a-SEP@LDH, a-SEP@LDH-PAMA in N_2

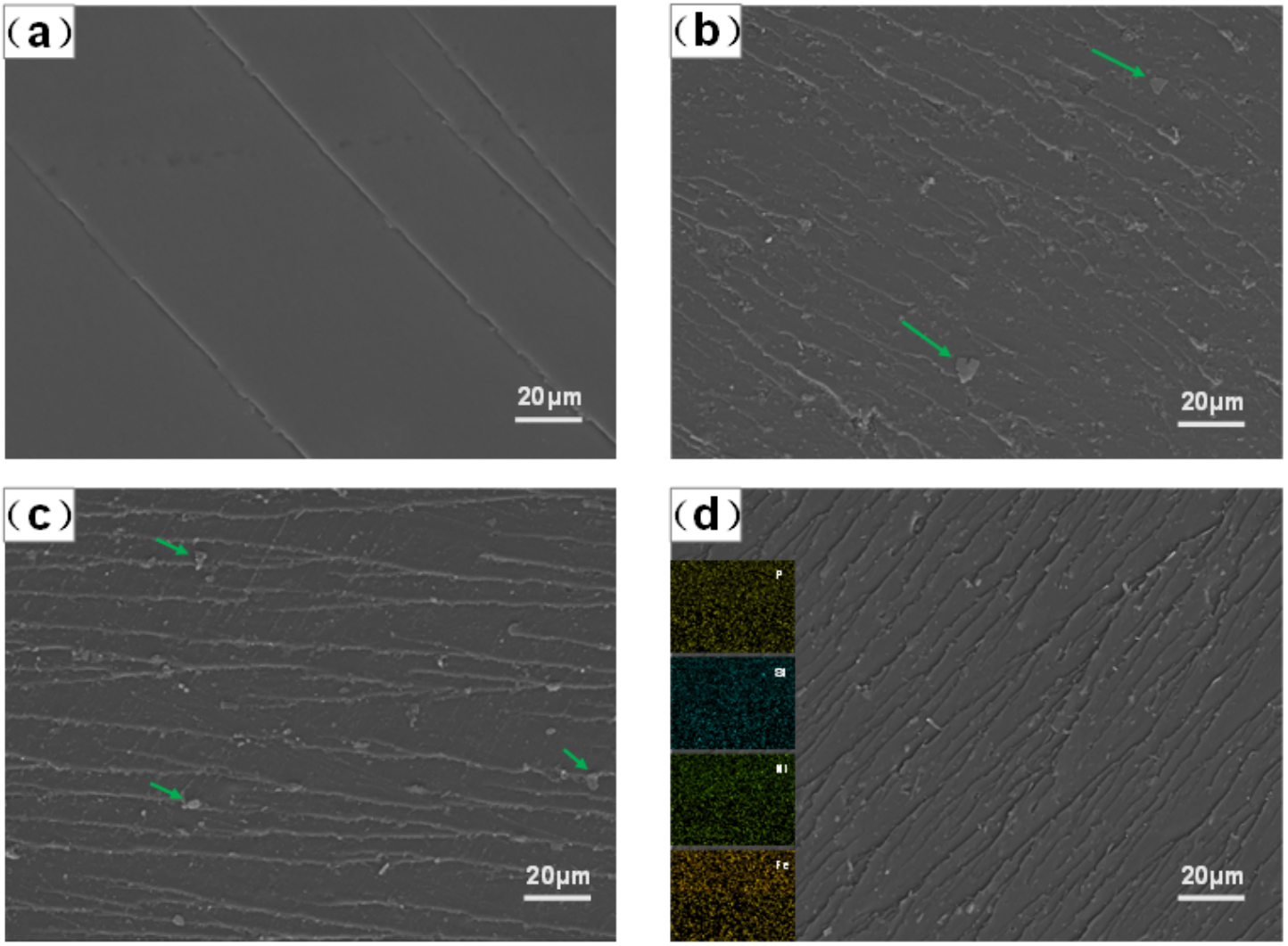


Figure 5

Fracture surface morphologies of (a) EP, (b) EP/PAMA, (c) EP/a-SEP@LDH, (d) EP/a-SEP@LDH/PAMA, the insets are element mapping images (P, Si, Ni, Fe) of EP/a-SEP@LDH/PAMA

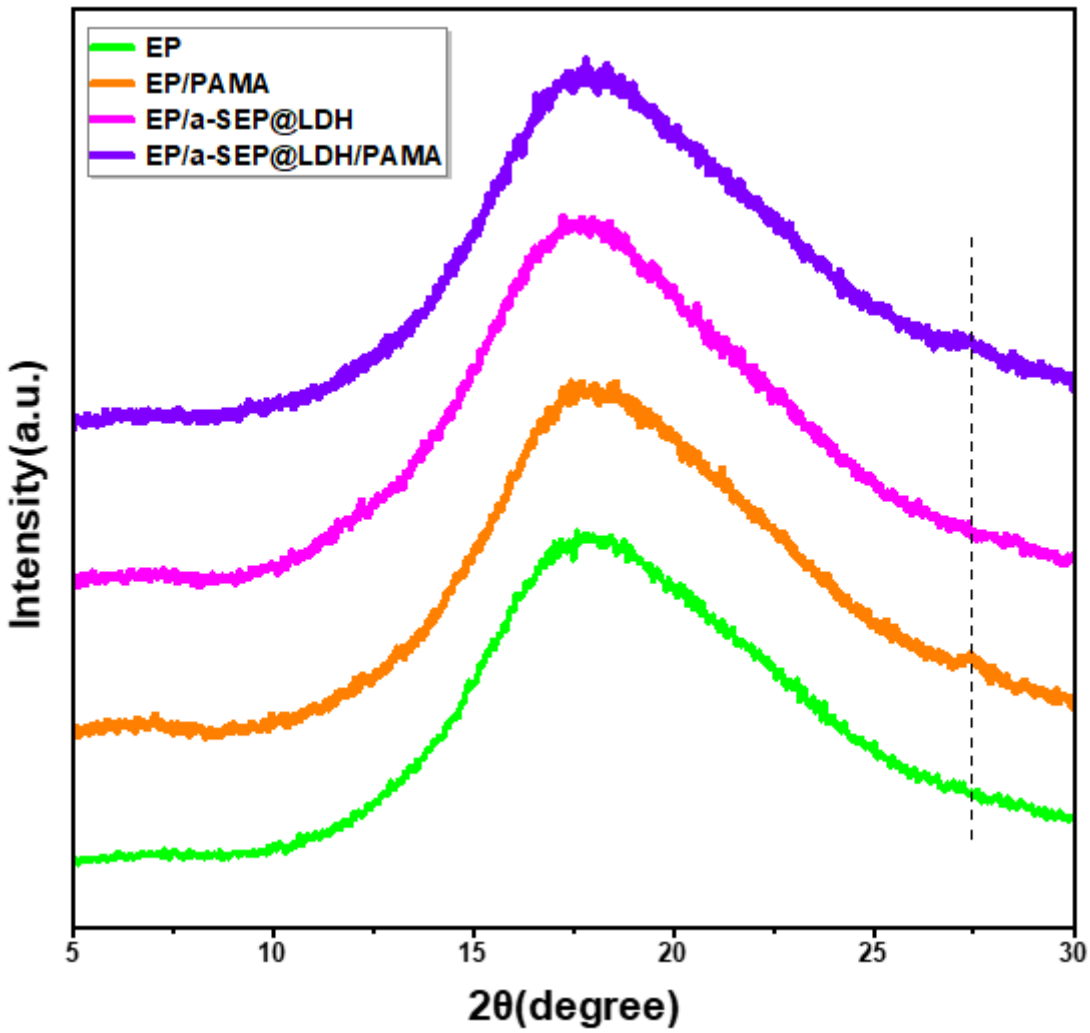


Figure 6

The XRD patterns of EP/PAMA, EP/LDH, EP/a-SEP-LDH and EP/a-SEP@LDH/PAMA

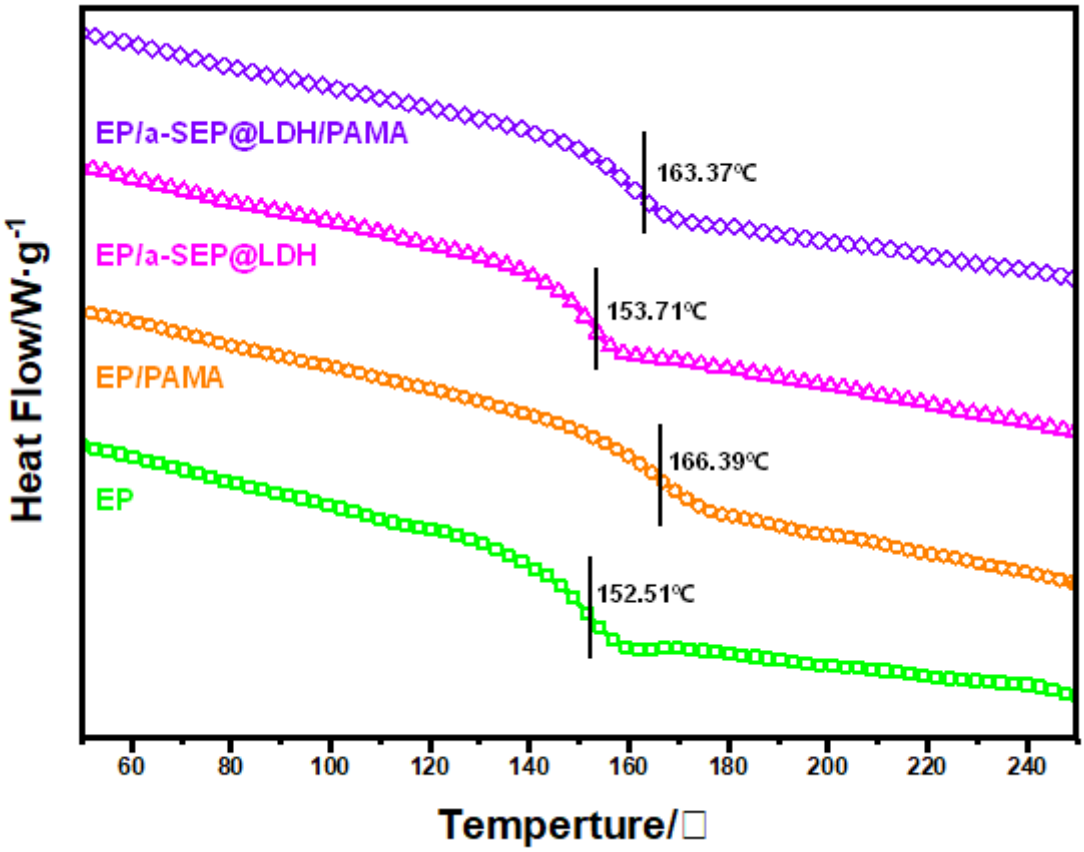


Figure 7

DSC curves of EP and EP composites

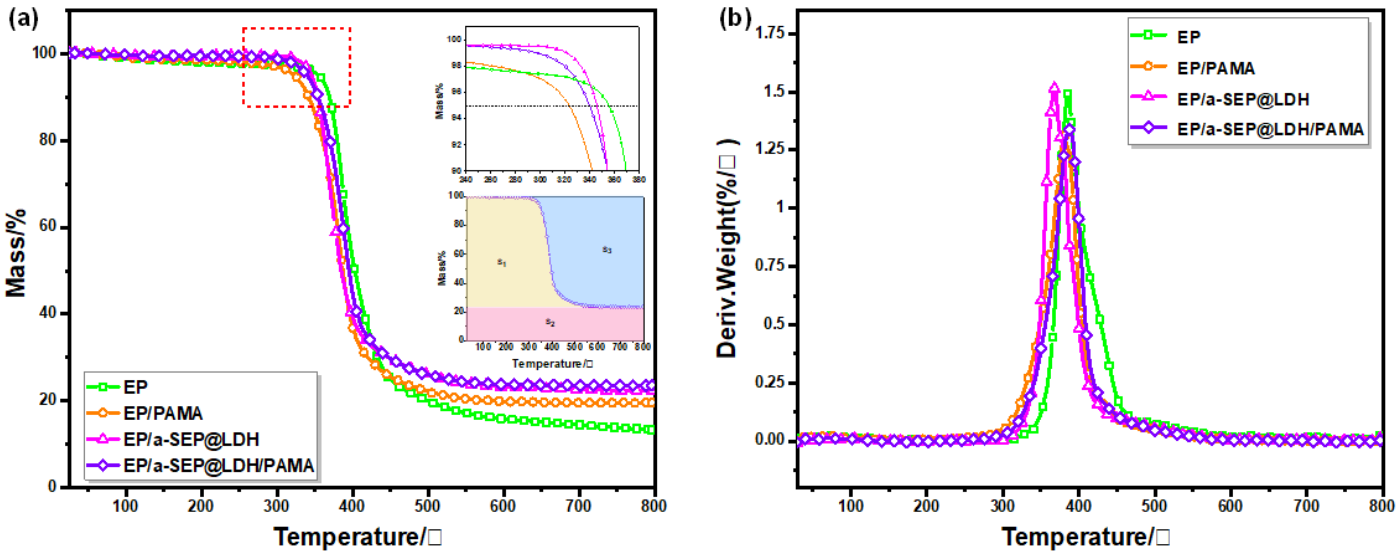


Figure 8

Thermal analysis of EP and its composites: (a) TG and the enlarged TG curves among

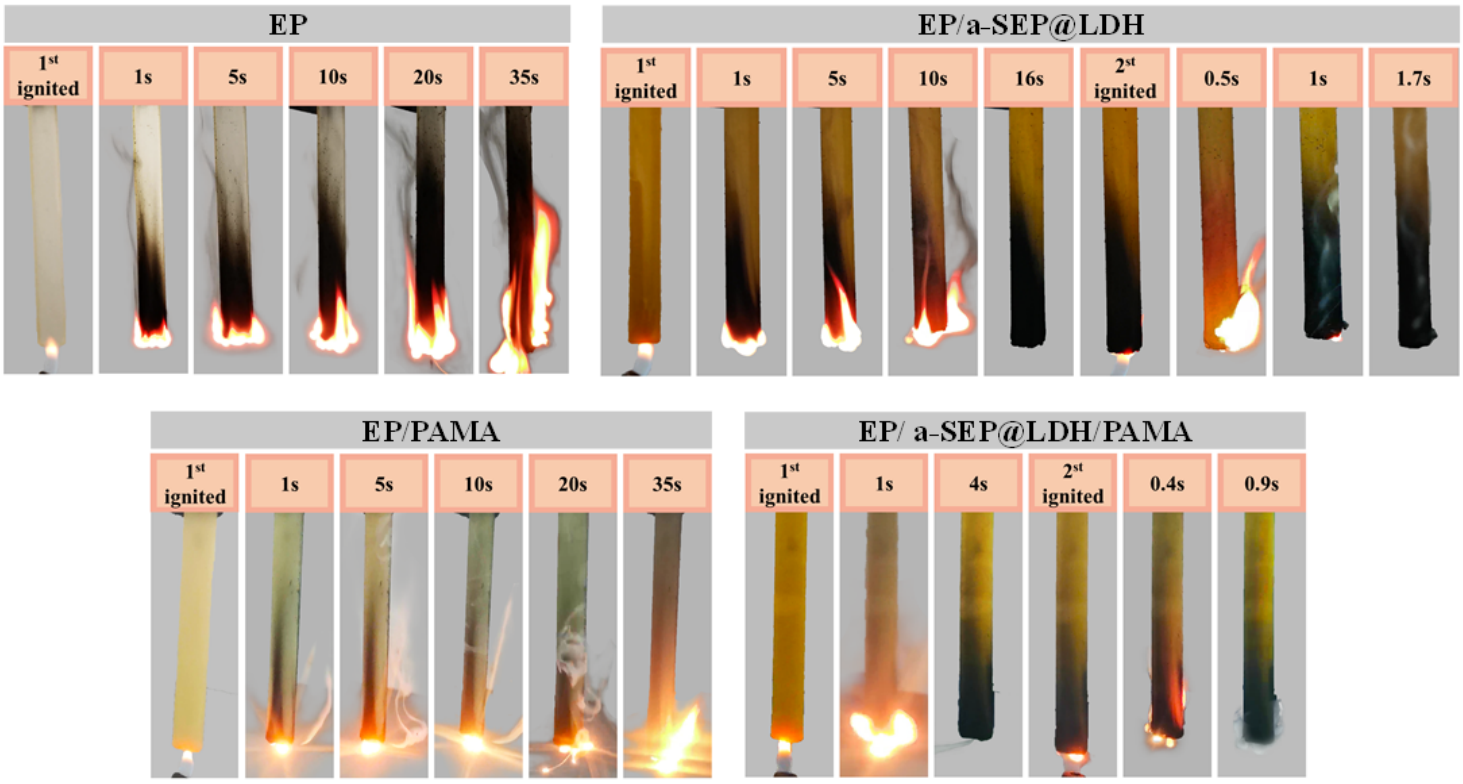


Figure 9

The video screenshots of EP and its composites in UL-94 test

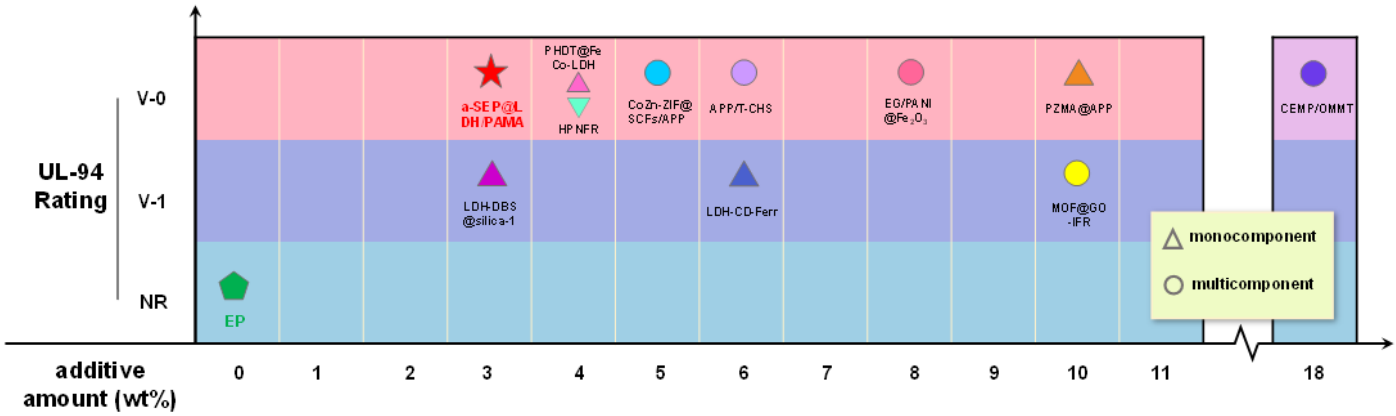


Figure 10

Comparison of additive amount and UL-94 rating of as-designed EP composites with the flame retardant EP reported previously

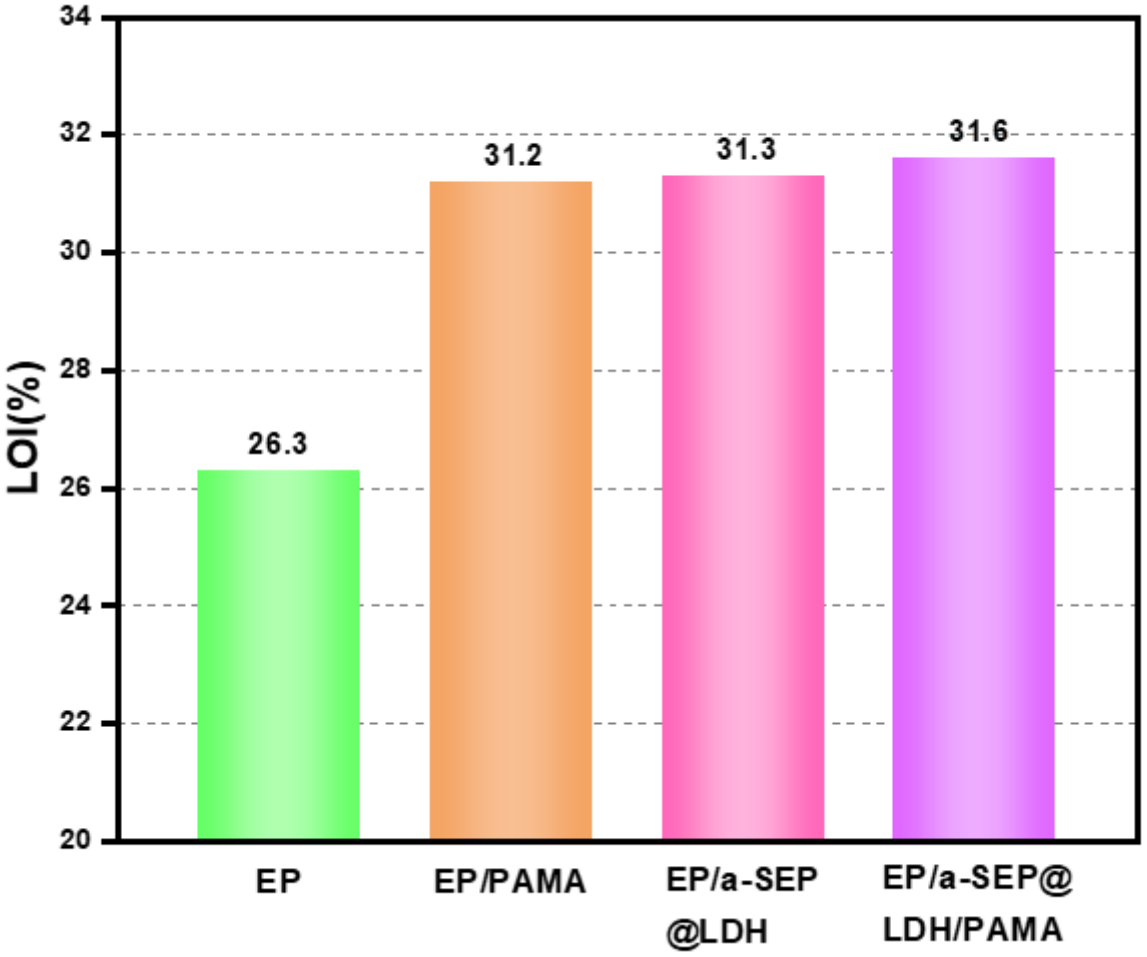


Figure 11

The LOI histogram of EP and its composites

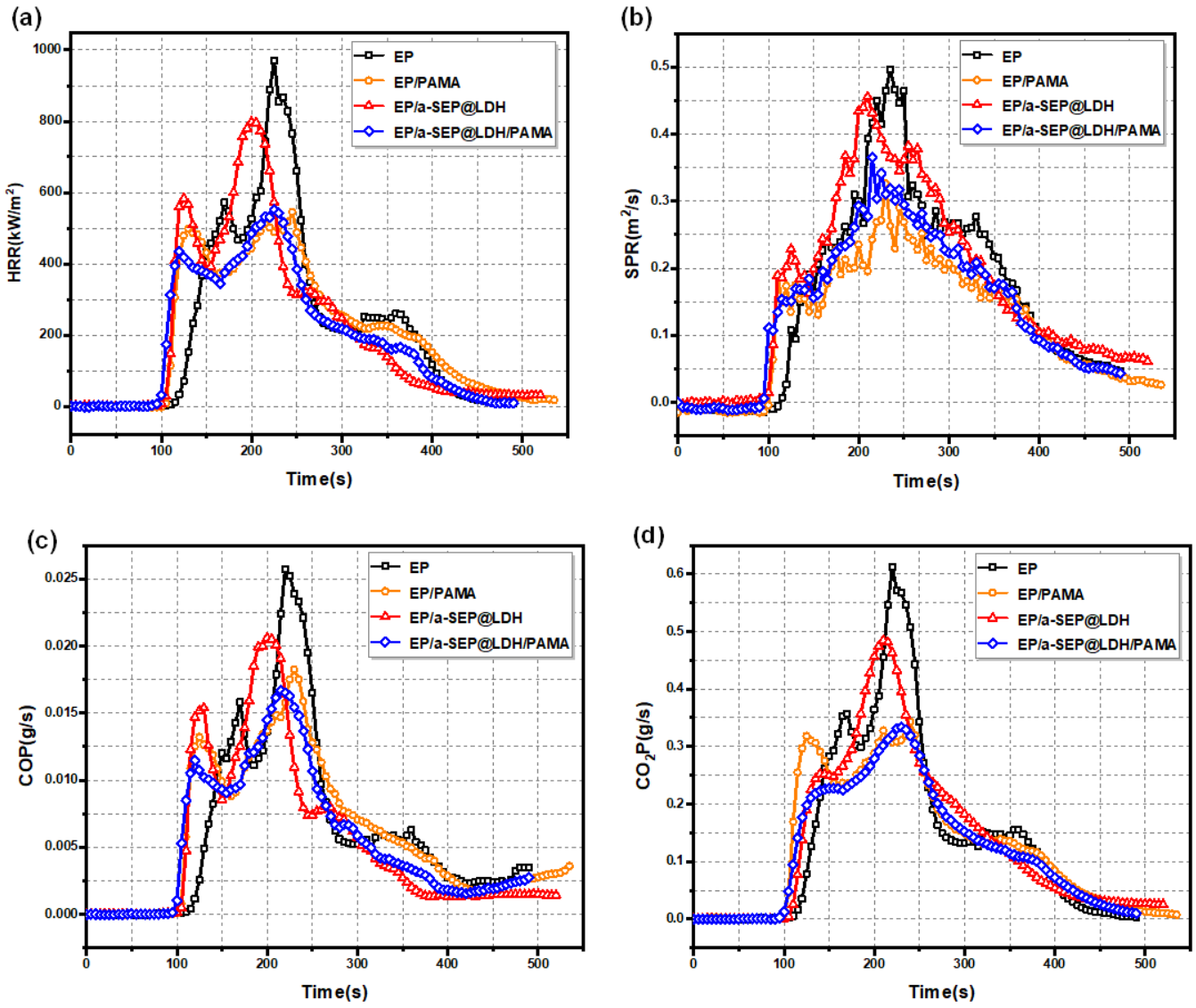


Figure 12

HRR (a), SPR (b), COP(c) and CO_2P (d) for EP and its composites

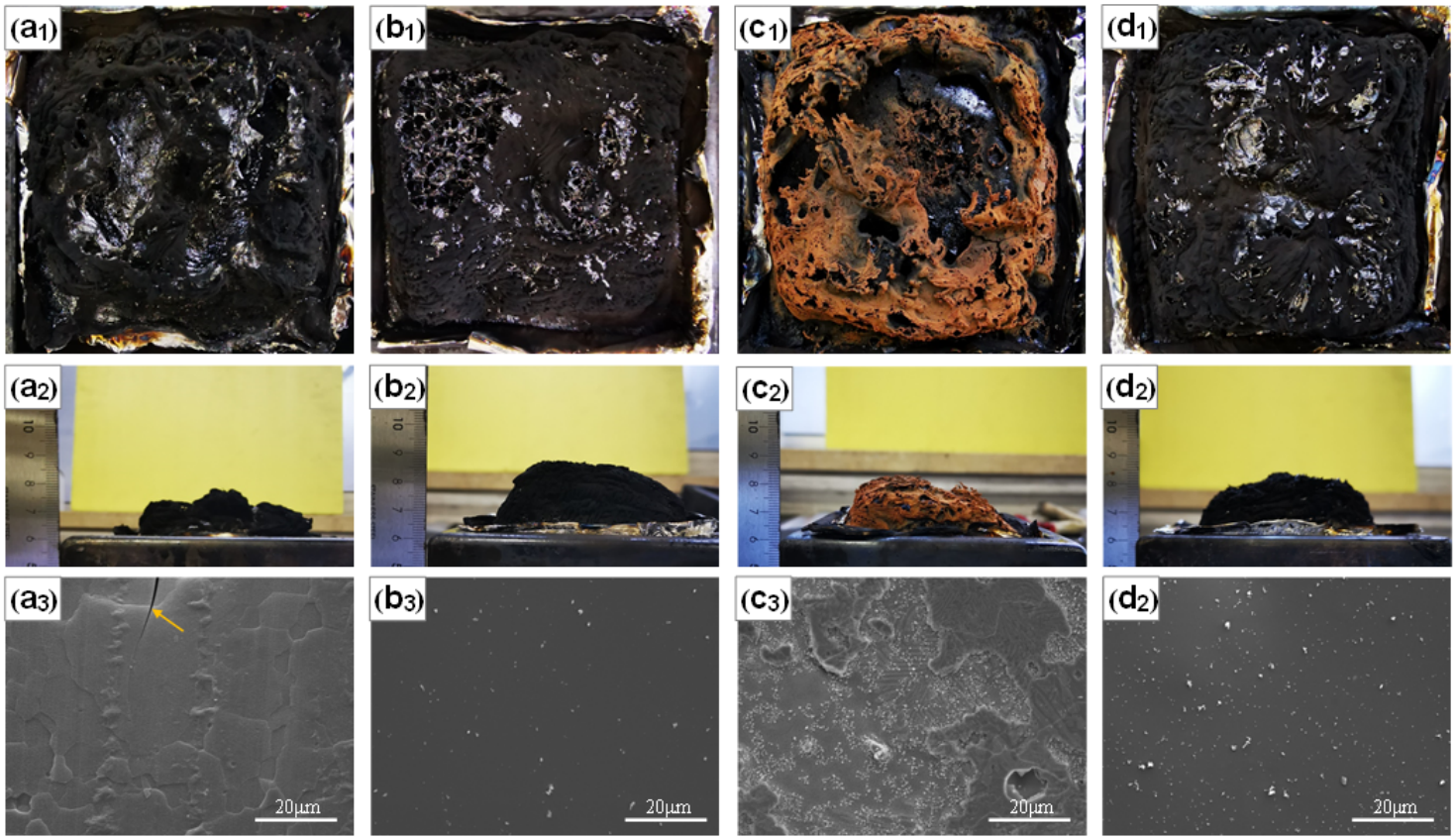


Figure 13

the digital photos of the char residue and the SEM micrograph of the interior char residue: EP(a_1, a_2, a_3), EP/PAMA(b_1, b_2, b_3), EP/a-SEP@LDH(c_1, c_2, c_3), EP/a-SEP@LDH/PAMA(d_1, d_2, d_3)

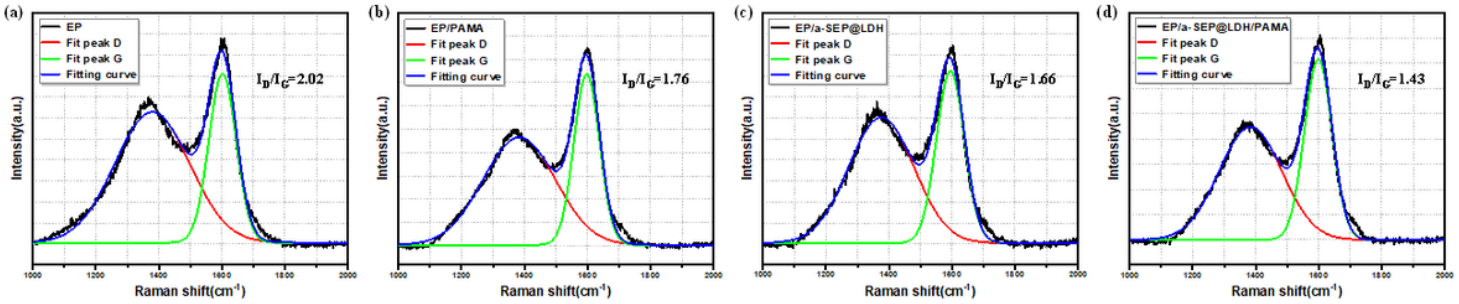


Figure 14

Raman spectra of the residual char after CCT test for (a) EP, (b) EP/PAMA, (c) EP/a-SEP@LDH and (d) EP/a-SEP@LDH/PAMA

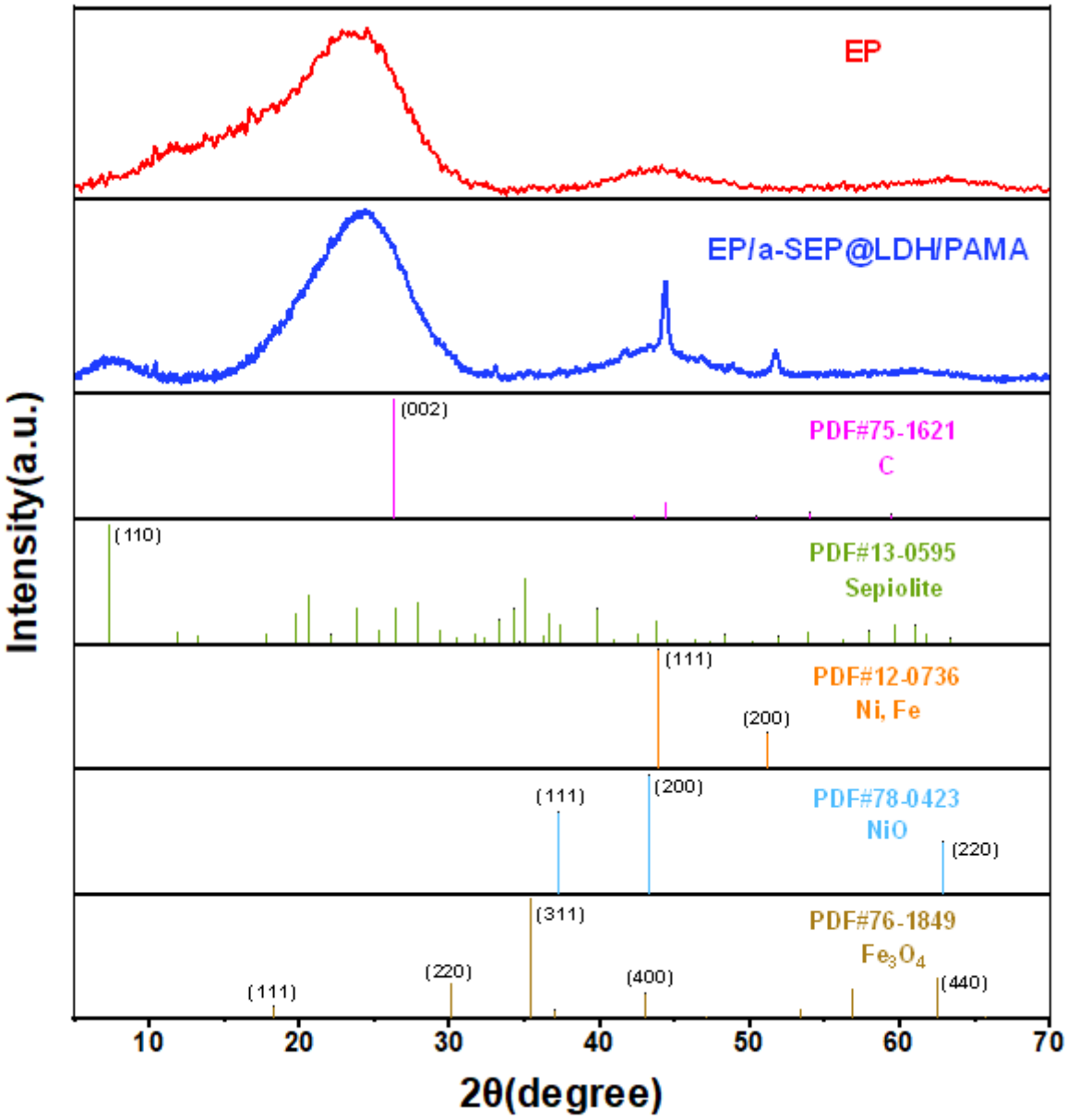


Figure 15

XRD patterns of the char residue after CCT test for EP and EP/a-SEP@LDH/PAMA

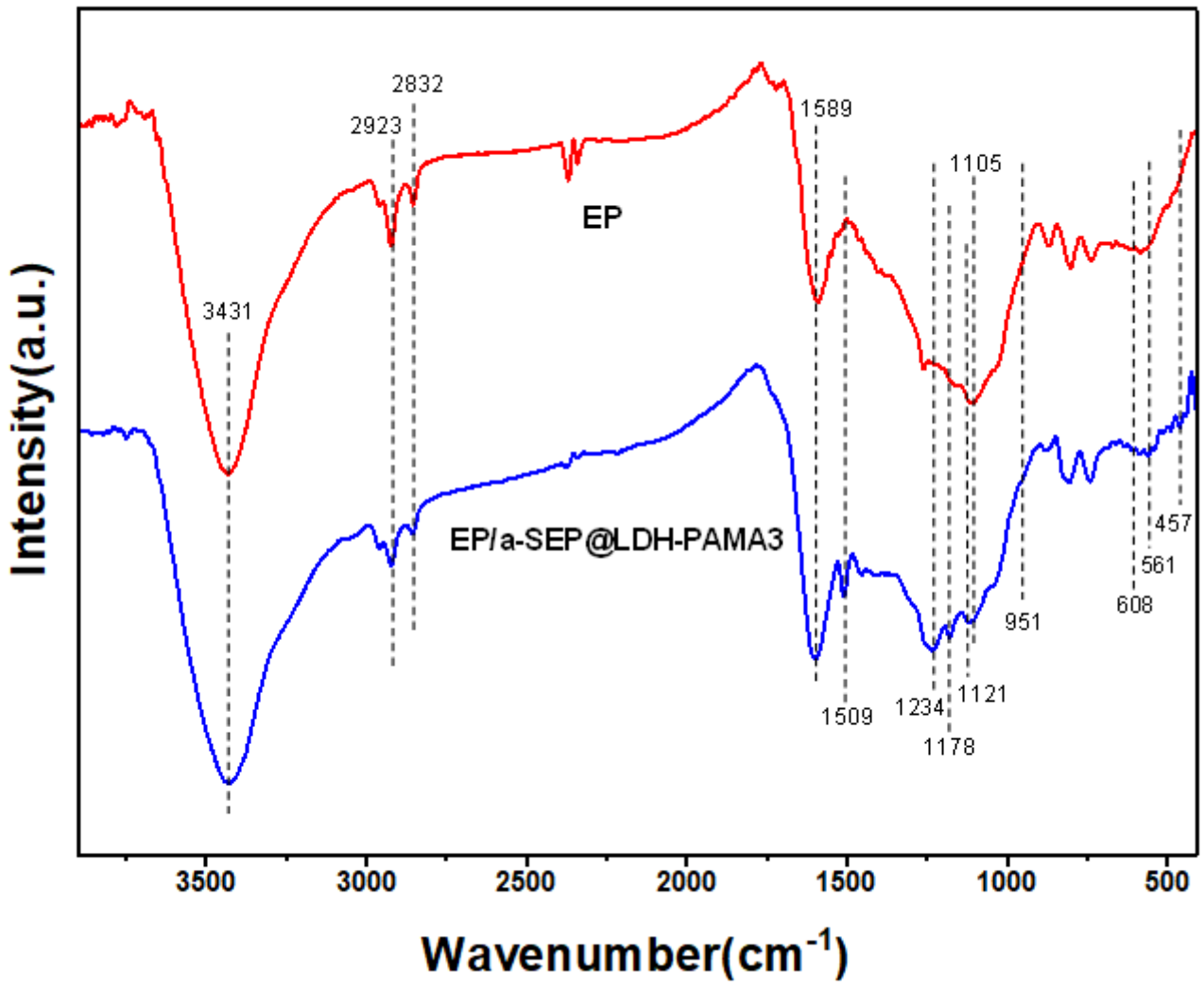


Figure 16

FTIR spectra of the residual char after CCT test for EP and EP/a-SEP@LDH/PAMA

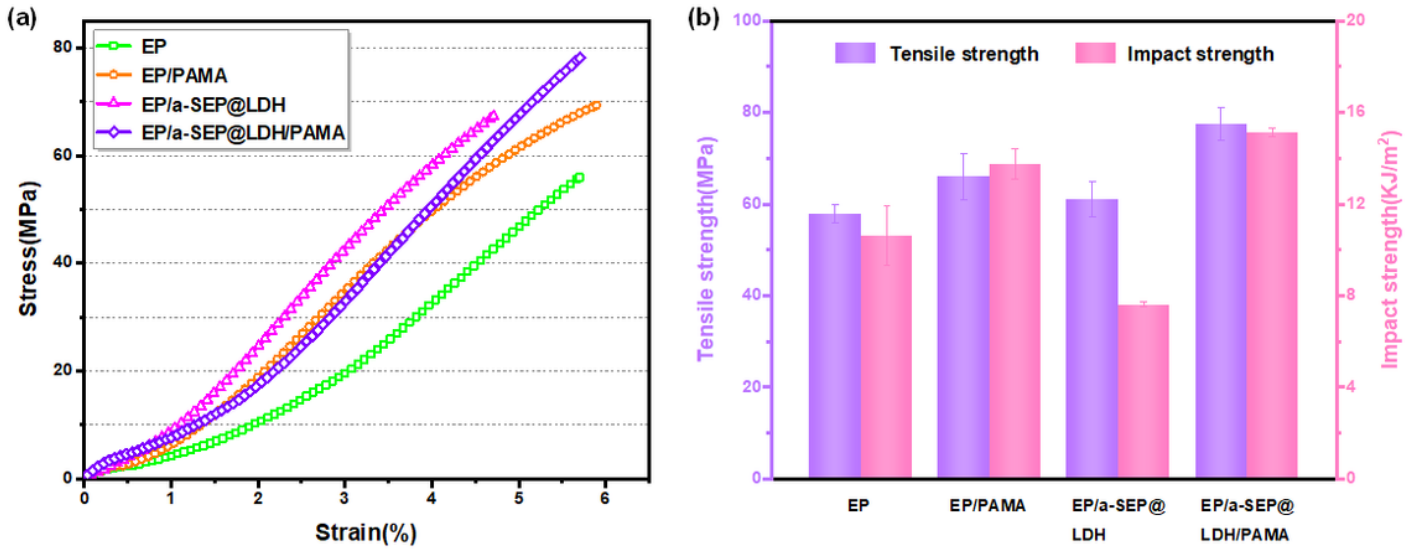


Figure 17

Stress-strain curves (a), tensile strength and impact strength (b) of EP and its composites

Supplementary Files

This is a list of supplementary files associated with this preprint. Click to download.

- scheme1.png
- Scheme2.png